

ENHANCEMENT OF AMMONIA GAS SENSING BY METAL OXIDE-POLYANILINE
NANOCOMPOSITE



A Thesis Submitted in Partial Fulfillment of the Requirements
for the Degree of Master of Science in Chemistry
Department of Chemistry
FACULTY OF SCIENCE
Chulalongkorn University
Academic Year 2022
Copyright of Chulalongkorn University

การเพิ่มสัญญาณการรับรู้แก๊สแอมโมเนียด้วยนาโนคอมพอสิตโพลีเอทิลีน-พอลิเอทิลีน



วิทยานิพนธ์นี้เป็นส่วนหนึ่งของการศึกษาตามหลักสูตรปริญญาวิทยาศาสตรมหาบัณฑิต

สาขาวิชาเคมี ภาควิชาเคมี

คณะวิทยาศาสตร์ จุฬาลงกรณ์มหาวิทยาลัย

ปีการศึกษา 2565

ลิขสิทธิ์ของจุฬาลงกรณ์มหาวิทยาลัย

ณัฐวุฒิ สร้อยบาง : การเพิ่มสัญญาณการรับรู้แก๊สแอมโมเนียด้วยนาโนคอมพอสิตโลหะออกไซด์-พอลิแอนิไลน์. (ENHANCEMENT OF AMMONIA GAS SENSING BY METAL OXIDE-POLYANILINE NANOCOMPOSITE) อ.ที่ปรึกษาหลัก : ผศ. ดร.เจริญขวัญ ไกรยา

แก๊สแอมโมเนีย (NH_3) เป็นสารเคมีที่สำคัญในหลายอุตสาหกรรม พนักงานที่ทำงานในเขตอุตสาหกรรมดังกล่าวอาจได้รับสัมผัสกับแก๊สแอมโมเนีย ซึ่งอาจทำให้เกิดอาการต่าง ๆ เช่น ระคายเคืองต่อผิวหนังและดวงตา และปัญหาในระบบทางเดินหายใจ โดยการพัฒนาตัวรับรู้แก๊สแอมโมเนียได้รับความสนใจอย่างมาก ในการศึกษาชิ้นนี้ เส้นใยนาโนทินไดออกไซด์ (SnO_2 NFs) ถูกประดิษฐ์ขึ้นด้วยการปั่นเส้นใยด้วยไฟฟ้าสถิต (electrospinning) เส้นใยนาโนทินไดออกไซด์ถูกผสมด้วยพอลิแอนิไลน์ (PANI) ซึ่งเป็นพอลิเมอร์นำไฟฟ้า เกิดเป็นทินไดออกไซด์-พอลิแอนิไลน์นาโนคอมพอสิต (SnO_2 NFs@PANI) ซึ่งลักษณะทางสัณฐานวิทยาของนาโนคอมพอสิตของตัวรับรู้ที่ได้รับนั้นได้รับการตรวจสอบด้วย SEM-EDS และ XRD จากนั้น SnO_2 NFs@PANI ได้รับการทดสอบและแสดงให้เห็นถึงการพัฒนาและการตรวจจับที่ดีสำหรับแก๊ส NH_3 ซึ่งรวมถึงความเป็นเส้นตรงของการตอบสนองต่อความเข้มข้นที่ดีในช่วง 0.4 - 100 ppm และมีขีดจำกัดการตรวจวัดที่ 12.4 ppb ที่อุณหภูมิห้อง นอกจากนี้ ตัวรับรู้นี้ยังมีอัตราการตอบสนองและการฟื้นตัวอย่างรวดเร็วที่ 87 วินาที และ 160 วินาที มีความจำเพาะเลือกต่อแก๊สแอมโมเนียที่ดี มีความสามารถในการทวนซ้ำที่ดี มีความเสถียรในระยะยาว และมีความสามารถในการทำซ้ำที่ดีสำหรับแอมโมเนียที่มีความเข้มข้น 10 ppm ที่อุณหภูมิห้อง นอกจากนี้ ยังมีการอภิปรายในรายละเอียดของกลไกการตรวจวัดแก๊สแอมโมเนียบน SnO_2 NFs@PANI ซึ่งลักษณะเฉพาะของการรับรู้ที่เพิ่มขึ้นของนาโนคอมพอสิตเกี่ยวข้องกับโครงสร้างทางสัณฐานวิทยาและ p-n heterojunction ระหว่าง PANI และ SnO_2 NF

สาขาวิชา เคมี
ปีการศึกษา 2565

ลายมือชื่อนิสิต
ลายมือชื่อ อ.ที่ปรึกษาหลัก

6270193923 : MAJOR CHEMISTRY

KEYWORD: Tin dioxide, Polyaniline, Ammonia, Sensor, Nanocomposite

Nattawut Soibang : ENHANCEMENT OF AMMONIA GAS SENSING BY METAL OXIDE-POLYANILINE NANOCOMPOSITE. Advisor: Asst. Prof. CHAROENKWAN KRAIYA, Ph.D.

Ammonia (NH₃) gas is an important chemical in many industries. Employees who work in those industrial areas may be exposed to a certain concentration of NH₃ which could cause various symptoms such as irritation of skin and eyes and problems in respiratory system. The development of new NH₃ sensing material has drawn a great attention. In this study, porous tin dioxide nanofibers (SnO₂ NFs) were successfully fabricated by an electrospinning technique. The SnO₂ NFs were composited with polyaniline (PANI), conducting polymer and form tin dioxide nanofibers@polyaniline nanocomposite (SnO₂ NFs@PANI). The morphology was characterized using SEM-EDS and XRD. The SnO₂ NFs@PANI was examined and showed improving and desirable sensing for NH₃ gas, which includes a good linearity response in a range of 0.4 - 100 ppm, and a detection limit of 12.4 ppb at room temperature. Furthermore, the present sensor also showed a rapid response and recovery rates of 87 s and 160 s, good selectivity, repeatability, long-term stability, and reproducibility to 10 ppm NH₃ at room temperature. Furthermore, the gas sensing mechanisms of NH₃ on SnO₂ NFs@PANI were also discussed in detail. The enhanced sensing characteristics of nanocomposites were related to the morphology structure and p-n heterojunction between PANI and SnO₂ NFs.

Field of Study: Chemistry

Student's Signature

Academic Year: 2022

Advisor's Signature

ACKNOWLEDGEMENTS

First of all, I would like to express my deepest gratitude to my advisor Assistant Professor Dr. Charoenkwan Kraiya for her constructive suggestion, consistent support and encouragement during the working on this research due to her kindness and empathy, I complete this thesis without a lot of difficulty.

Furthermore, I would also like to thank Professor Dr. Patchanita Thamyongkit, Assistant Professor Dr. Puttaruksa Varanusupakul, and Dr. Eakkasit Punrat for their helpful recommendations.

In addition, I would like to thank the Electrochemistry and Optical Spectroscopy Center of Excellence, Department of Chemistry, Faculty of Science, Chulalongkorn University for the financial support and for supplying some chemicals in this research.

Finally, I would like to thank every person who has passed through my life in these three and a half years and made it a wonderful time.

Nattawut Soibang

TABLE OF CONTENTS

	Page
ABSTRACT (THAI).....	iii
ABSTRACT (ENGLISH).....	iv
ACKNOWLEDGEMENTS.....	v
TABLE OF CONTENTS.....	vi
LIST OF TABLES.....	x
LIST OF FIGURES.....	xii
LIST OF ABBREVIATIONS.....	xiv
CHAPTER 1 INTRODUCTION.....	1
1.1 Problem Definition.....	1
1.2 Objectives.....	3
1.3 Scope of thesis.....	3
CHAPTER 2 THEORY.....	4
2.1 Electrospinning technique.....	4
2.2 Conducting polymers.....	7
2.3 CPs-metal oxide composite for gas sensing.....	8
2.4 Mechanism of tin dioxide nanofibers@polyaniline nanocomposite (SnO ₂ NFs@PANI) to NH ₃	9
2.5 Response, response time and recovery time.....	10
2.6 Properties of gas-sensing material.....	11
2.7 NH ₃ gas sensor.....	11
CHAPTER 3 EXPERIMENTAL.....	13

3.1 Instruments and apparatus	13
3.2 Chemicals and materials	13
3.3 Preparation of SnO ₂ nanofibers by electrospinning technique	14
3.4 Synthesis of NH ₃ -sensing materials.....	15
3.4.1 Pure polyaniline (PANI)	15
3.4.2 SnO ₂ /PANI	16
3.4.3 SnO ₂ NFs@PANI.....	16
3.5 Fabrication of screen-printed electrode.....	16
3.6 Sensor fabrication.....	17
3.6.1 Types of sensing material	17
3.6.2 Types of substrates	17
3.6.3 Numbers of drop-casting layer.....	17
3.6.4 Concentration of SnO ₂ NFs@PANI in DMF solution	18
3.7 Performance of NH ₃ sensor.....	18
3.7.1 Linear range and limit of detection	20
3.7.2 Selectivity	20
3.7.3 Repeatability	20
3.7.4 Reproducibility.....	20
3.7.5 Long-term stability.....	20
3.7.6 Application of the SnO ₂ NFs@PANI sensor in fish freshness evaluation....	21
CHAPTER 4 RESULTS & DISCUSSION	22
4.1 Preparation of SnO ₂ nanofibers by electrospinning.....	22
4.1.1 Type of polymer and its percentage	22
4.1.2 Percentage of SnCl ₂ · 2H ₂ O in the nanofibers.....	24

4.1.3	Types of collectors in electrospinning	25
4.1.4	Characterization of SnO ₂ nanofibers	26
4.2	<i>In-situ</i> polymerization of SnO ₂ NFs in PANI.....	27
4.2.1	Weight of SnO ₂ NFs in PANI	28
4.2.2	Time for <i>in-situ</i> polymerization.....	29
4.2.3	Filtration method for SnO ₂ NFs@PANI synthesis process result diagnosis: vacuum pump and gravity.....	31
4.2.4	Characterization of SnO ₂ NFs@PANI.....	33
4.3	Sensor fabrication.....	35
4.3.1	Types of sensing material and their response-recovery times.....	35
4.3.2	Types of substrates	37
4.3.3	Number of drop-casting layers.....	39
4.3.4	Concentration of SnO ₂ NFs@PANI in DMF solution	41
4.4	Performance of NH ₃ sensor.....	43
4.4.1	Linear range and limit of detection	43
4.4.2	Selectivity	44
4.4.3	Repeatability and long-term stability	45
4.4.4	Reproducibility.....	46
4.4.5	Sample analysis.....	47
4.4.6	Summary of NH ₃ sensing parameters for PANI-metal oxide-based sensing systems.....	49
CHAPTER 5 CONCLUSION		51
REFERENCES		52
VITA.....		64



จุฬาลงกรณ์มหาวิทยาลัย
CHULALONGKORN UNIVERSITY

LIST OF TABLES

	Page
Table 2.1 Required and undesired properties of gas-sensing material.....	11
Table 2.2 Currently available NH ₃ gas sensors with their properties.....	12
Table 4.1 Types and percentages of polymer for nanofibers formation by electrospinning.....	23
Table 4.2 Percentages of SnCl ₂ · 2H ₂ O in the nanofiber formation by electrospinning.....	24
Table 4.3 Types of collectors in electrospinning for nanofibers formation.....	25
Table 4.4 Responses of the SnO ₂ NFs@PANI composites, prepared from different weight of SnO ₂ NFs to 10 ppm NH ₃	29
Table 4.5 Response of polymerize time to prepare the SnO ₂ NFs@PANI composite..	30
Table 4.6 t-test value of polymerize time to prepare the SnO ₂ NFs@PANI composite.....	31
Table 4.7 Response of filtration method of filters used at the end of SnO ₂ NFs@PANI polymerization.....	32
Table 4.8 t-test value of filtration method of filters used at the end of SnO ₂ NFs@PANI polymerization.....	33
Table 4.9 Response of types of sensing material.....	36
Table 4.10 Response of types of substrates.....	38
Table 4.11 Response of drop-casting layers.....	40
Table 4.12 Ratio of response vs. preparation times.....	41
Table 4.13 Response of concentration of SnO ₂ NFs@PANI in DMF solution.....	42
Table 4.14 Response of fabricated sensor (reproducibility test).....	47

Table 4.15 Sensing performance of the recently reported NH ₃ gas sensors base on PANI-metal oxide in advanced techniques.	50
---	----



LIST OF FIGURES

	Page
Figure 1.1 Effects of ammonia gas exposure.	1
Figure 1.2 Schematic illustration of the interaction of NH ₃ gas with PANI occurring at the continuous chain (N) on the polymer structure.	3
Figure 2.1 Basic setup for electrospinning.	4
Figure 2.2 Applications of electrospinning.	6
Figure 2.3 Schematic illustration of applications of conducting polymers and their composites.	7
Figure 2.4 Resistance transient of an n-type gas sensor shows stable resistance in air (R _a), stable resistance in gas (R _g), response time (t _{res}), and recovery time (t _{rec}).	10
Figure 3.1 Scheme of electrospinning technique for preparation of SnO ₂ NFs.	15
Figure 3.2 Screen-printed electrode for NH ₃ sensors.	16
Figure 3.3 In-house gas detector.	19
Figure 3.4 The response and recovery times.	19
Figure 4.1 SEM images and EDS mapping of (A) PAN/SnCl ₂ nanofibers and (B) SnO ₂ nanofibers.	27
Figure 4.2 XRD patterns of (A) PAN/SnCl ₂ nanofibers and (B) SnO ₂ nanofibers.	27
Figure 4.3 10 ppm NH ₃ gas responses on 1, 2, 4, and 7 mg SnO ₂ NFs that was composited with PANI and was, then, cast on SPGE.	28
Figure 4.4 10 ppm NH ₃ gas responses on 0.5, 1, 2, 4, and 6 hrs. polymerize time for 2 mg SnO ₂ NFs composited with PANI and was, then, cast on SPGE.	30
Figure 4.5 10 ppm NH ₃ gas responses on vacuum pump (blue) and gravity (orange) for SnO ₂ NFs@PANI composite.	32
Figure 4.6 SEM images and EDS mapping of SnO ₂ NFs@PANI.	34

Figure 4.7 XRD patterns of (A) PANI, (B) SnO ₂ NFs and (C) SnO ₂ NFs@PANI.....	34
Figure 4.8 Responses, response times, and recovery times of 0.6 ppm NH ₃ measured by pure PANI (green line), SnO ₂ /PANI (blue line), and SnO ₂ NFs/PANI (yellow line) sensing materials cast on SPCE.....	36
Figure 4.9 Responses of 0.6 ppm NH ₃ measured by 1 mg SnO ₂ NFs@PANI cast on acrylic (grey line), ceramic (orange line), SPCE (yellow line) and SPGE (blue line).	38
Figure 4.10 Contact angle of a DMF drop containing sensing material on difference substrate: A) SPGE, B) SPCE, C) ceramic, and D) acrylic.....	39
Figure 4.11 Responses of 10 ppm NH ₃ measured by 2 mg SnO ₂ NFs@PANI cast on SPGE with 2 layers (blue line), 4 layers (orange line), 6 layers (grey line), 8 layers (yellow line) and 10 layers (green line) drop casting.....	40
Figure 4.12 Responses of 10 ppm NH ₃ measured by 1 mg (blue line), 2 mg (orange line), 5 mg (yellow line), and 7 mg (grey line) SnO ₂ NFs@PANI cast on SPGE.....	42
Figure 4.13 A) Dynamic response of the SnO ₂ NFs@PANI sensor to 0.4 - 100 ppm NH ₃ gas. B) Response of the SnO ₂ NFs@PANI sensor as a function of NH ₃ concentration at room temperature.....	44
Figure 4.14 Selectivity responses of 10 ppm NH ₃ , acetone, ethanol, formaldehyde, methanol, and toluene gases at room temperature.....	45
Figure 4.15 A) Ten repeatedly responses. B) Long-term stability of the SnO ₂ NFs@PANI sensor response to 10 ppm NH ₃ gas at room temperature.....	46
Figure 4.16 Reproducibility response of five SnO ₂ NFs@PANI sensors to 10 ppm NH ₃ gas at room temperature.....	47
Figure 4.17 NH ₃ contents in fish sample detected by the SnO ₂ NFs@PANI sensor.....	48

LIST OF ABBREVIATIONS

°C	Degree Celsius
AC	Alternating current
Al ₂ O ₃	Aluminum oxide
APS	Ammonium peroxydisulphate
C	Concentration
C ₃ H ₆ O	Acetone
C ₆ H ₅ CH ₃	Toluene
CH ₂ O	Formaldehyde
CH ₃ CH ₂ OH	Ethanol
Co ₃ O ₄	Cobalt tetraoxide
CPs	Conductive polymers
DC	Direct current
DMF	Dimethylformamide
EB	Emeraldine base
ES	Emeraldine salt
HCl	Hydrochloric acid
In ₂ O ₃	Indium oxide
LOD	Limit of detection
NH ₃	Ammonia
OSHA	Occupational Safety & Health Administration

PA	Polyacetylene
PAN	Polyacrylonitrile
PANI	Polyaniline
PCL	Poly(caprolactone)
PEDOT	Poly(3,4-ethylenedioxythiophene)
PLA	Poly (lactic acid)
PLGA	Poly (lactic-co-glycolic acid)
PPV	Poly(phenylene vinylene)
PPy	Polypyrrole
PS	Polystyrene
PT	Polythiophene
PVC	Poly (vinyl chloride)
PVP	Polyvinylpyrrolidone
R^2	Correlation coefficient
R_a	Stable resistance in air
R_g	Stable resistance in gas
S	Response
SEM-EDS	Scanning electron microscope/energy dispersive spectroscopy
$\text{SnCl}_2 \cdot 2\text{H}_2\text{O}$	Tin(II) chloride dihydrate
SnO_2 NFs@PANI	Tin dioxide nanofibers@polyaniline nanocomposite

SnO_2	Tin dioxide
SPCE	Screen-print carbon electrode
SPGE	Screen-print graphene electrode
TiO_2	Titanium dioxide
t_{rec}	Recovery time
t_{res}	Response time
XRD	X-Ray Diffraction



CHAPTER 1

INTRODUCTION

1.1 Problem Definition

Ammonia (NH_3) gas is an inorganic compound with pungent smell, classified as toxic gas that corrosive to some materials. The gas affects living organisms and is dangerous to humans. Ammonia gas is an important chemical resource in many chemical industries such as fertilizer production industry, automobile industry, cleaning products industry, pharmaceutical industry, plastic and polymer manufacturing industry and herbicide manufacturing industry. Employees who work in such industrial area are at risk to be exposed to some concentration of NH_3 for a long-term which may cause various symptoms such as irritation of skin and eyes and problems in respiratory system as showed in Figure 1 (Arasu et al., 2017). In atmosphere, the ammonia presents lower than 1-5 ppb (Pandeewari et al., 2022). According to the Occupational Safety & Health Administration (OSHA), human exposure to ammonia gas should not exceed 8 hrs and 15 mins when the concentrations are 25 ppm and 35 ppm (Pandeewari et al., 2022), respectively.

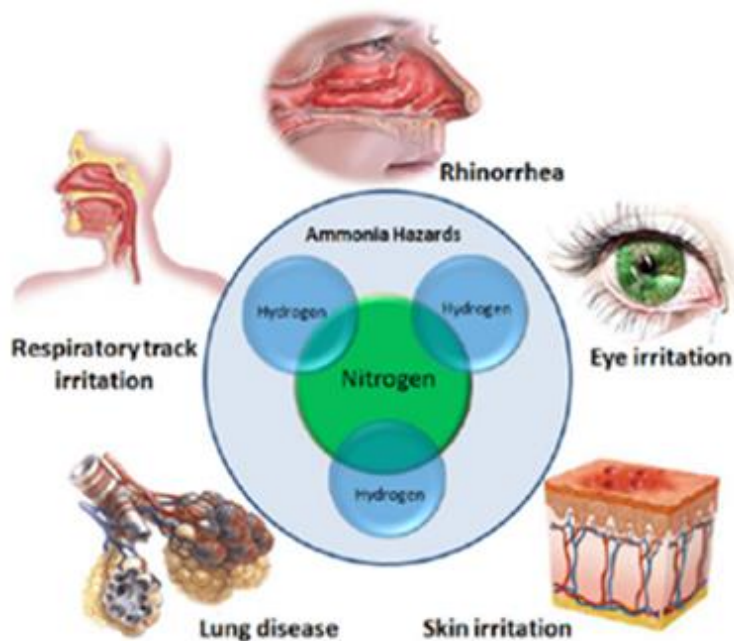


Figure 1.1 Effects of ammonia gas exposure.

The ammonia gas can be detected by many of spectroscopic methods (Hodgkinson & Tatam, 2013; Warland et al., 2001; Webber et al., 2001) or solid-state sensing methods (Balint et al., 2014; Huang et al., 2009; Janata & Josowicz, 2003; Kim & Lee, 2014; Kwak et al., 2019). Among those methods, solid-state probe composed of conducting polymer film made of polyaniline (PANI) (Bandgar, Navale, Nalage, et al., 2015; Kumar et al., 2017; Srový et al., 2016) polypyrrole (PPy) (Su et al., 2009) or poly(3,4-ethylenedioxythiophene) (PEDOT) (Kwon et al., 2010), is widely employed for the measurement at room temperature because the device is inexpensive and easy-to-handle. Although, those conducting polymers yield a fair sensitivity to NH_3 gas, their sensitivity and efficiency can be improved when functionalized with metal oxide (Das & Sarkar, 2017; He et al., 2020).

The use of polyaniline with metal oxides such as cobalt tetraoxide (Co_3O_4) (Feng et al., 2016), indium oxide (In_2O_3) (Li, Diao, et al., 2018) or titanium dioxide (TiO_2) (Liu et al., 2017) caused a change in properties in terms of stability, sensitivity or analysis limits. Tin dioxide (SnO_2) is an attractive metal oxide as it has a relatively wide energy band gap of 3.6 eV, low cost in the synthesis process and the synthesis reaction was not severe (Bera et al., 2018). Based on these properties of SnO_2 , it is suitable to be used in coordination with PANI.

In this work, SnO_2 and PANI are of interest. The PANI, showed in Figure 1.2, is a conducting polymer that can electrically exchange charges with NH_3 gas (Chatterjee et al., 2013). Its resistance alters when NH_3 gas presents. For SnO_2 , is an interesting metal because it is an n-type semiconductor, and it has wide energy band gap at 3.6 eV which resulting in good thermal stability. It is not only low-cost and easy to synthesize but it also an electrochemically favor (Bera et al., 2018; Hoa et al., 2010; Nie et al., 2018; Van Hieu, 2010). A previous work (Li et al., 2016) has reported fabrication method for SnO_2 doped in PANI by using a drop casting method, which is an easy method with less chemical waste. However, the ratio of surface area and quantity is low, and its characteristic is difficult to control. This research is interested in applying an electrospinning technique to control the dispersion of tin dioxide and to increase the surface area of PANI. Due to the technique, it is easy to control the fabrication of the fiber length and the pore structure.

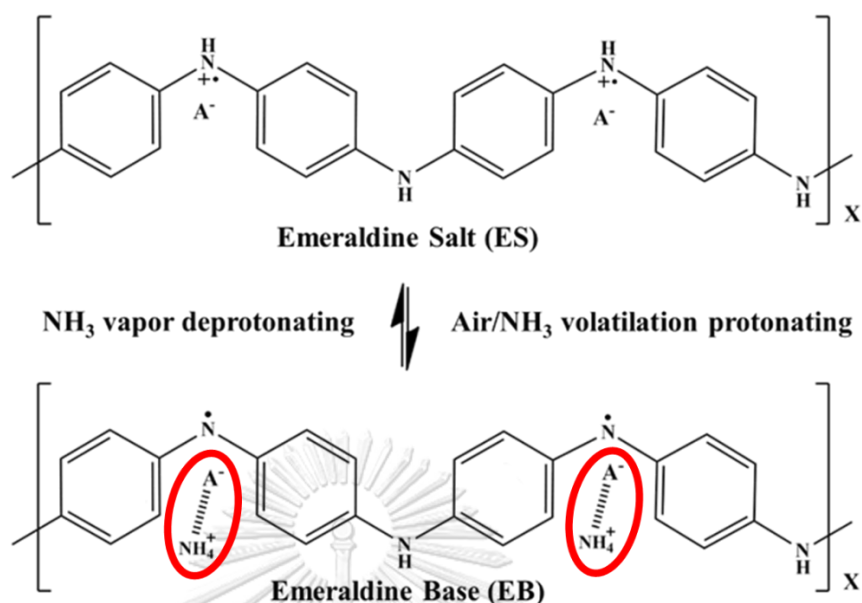


Figure 1.2 Schematic illustration of the interaction of NH_3 gas with PANI occurring at the continuous chain (N) on the polymer structure.

1.2 Objectives

1. To fabricate SnO_2 NFs using the electrospinning technique and modified with polyaniline
2. To study the efficiency of the SnO_2 NFs modified with PANI for using as ammonia gas sensors.

จุฬาลงกรณ์มหาวิทยาลัย
CHULALONGKORN UNIVERSITY

1.3 Scope of thesis

1. SnO_2 NFs were fabrication by an electrospinning technique.
2. The prepared SnO_2 NFs were characterized by SEM-EDS and XRD.
3. SnO_2 NFs were modified with PANI by *in-situ* polymerization method.
4. The prepared SnO_2 NFs modified with PANI were applied for using as ammonia gas sensors.

CHAPTER 2

THEORY

2.1 Electrospinning technique

Electrospinning is an electrohydrodynamic method that a liquid droplet is electrically activated to generate fibers from various type of materials. The simple setup for the major component of this electrospinning (Figure 2.1) (Rim et al., 2013) including (1) a high-voltage power supply which can be either direct current (DC) or alternating current (AC), (2) a syringe pump, and (3) a conductive collector.

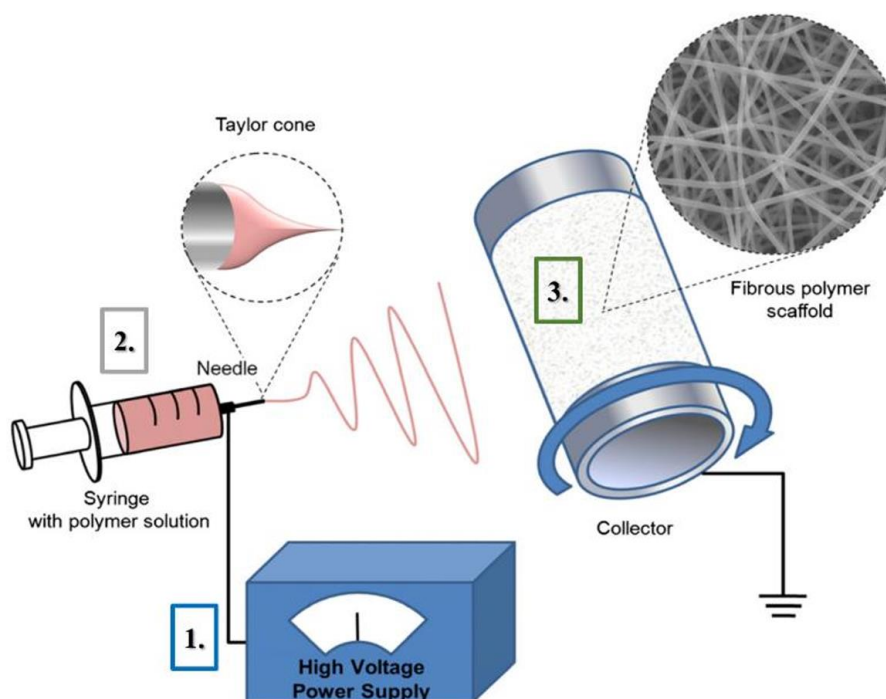


Figure 2.1 Basic setup for electrospinning.

In terms of the substance for electrospinning, it mostly is organic polymers in liquid form. Organic polymers can be divided into two types which are natural polymers and synthetic polymers. These polymers have different applications. Natural polymers such as DNA, silk fibroin, chitin, and chitosan, have been utilized to be a substrate to modify sensing materials. Synthetic polymers can be classified into

normal synthetic, biocompatible/biodegradable synthetic, and conductive synthetic polymers. Normal synthetic polymers such as polystyrene (PS) and poly (vinyl chloride) (PVC) can be commercially applied to environmental protection. Biocompatible/biodegradable synthetic polymers such as poly(caprolactone) (PCL), poly (lactic acid) (PLA), and poly (lactic-co-glycolic acid) (PLGA) can be further explored as scaffolds for biomedical applications. Conductive synthetic polymers such as polyaniline (PANI) and polypyrrole (PPy), have been utilized as sensing materials (Li & Xia, 2004; Xue et al., 2017).

A high-voltage power supply of 10–20 kV is often used with 5-15 cm distance between the needle and the collector (Figure 2.1). This technique is called far-field which produce thin fibers using simple apparatus. It is useful for mass production (Fuh & Hsu, 2011; Xiang Wang et al., 2012).

Using a needles in electrospinning, it produces nanofibers at a low throughput, typically 1–5 mL/h by flow rate or 0.1–1.0 g/h by fibers mass (Valipouri, 2017). This increases the productivity and emanated nanofibers (Liu et al., 2015).

The conductive solid collector can be used in stationary and movable modes. Movable mode is known as rotating collector (Matthews et al., 2002; Persano et al., 2013). Increasing the rotating speed decreases the diameter of the nanofibers due to the stretching force (Alfaro De Prá et al., 2017).

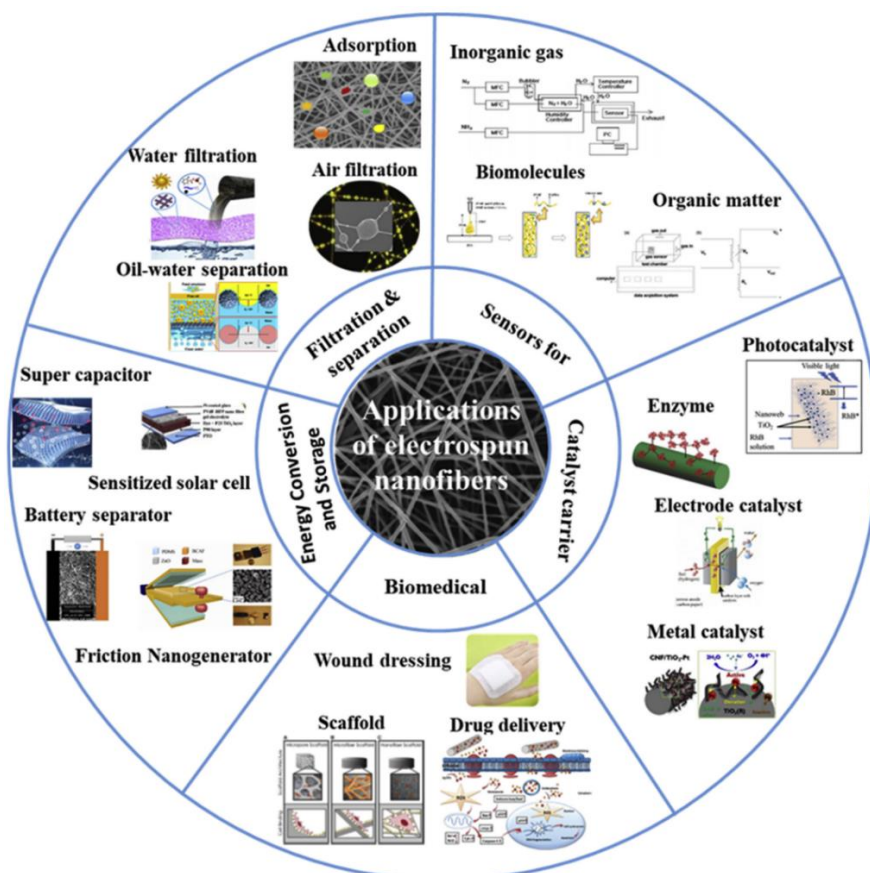


Figure 2.2 Applications of electrospinning.

Figure 2.2 displays a chart of nanofibers applications (Liu et al., 2020) as scaffolds (Bao et al., 2016; Ma et al., 2012), filters (Ge et al., 2018; Qayum et al., 2019), membranes (Chen et al., 2013), energy conversion and storage (Bandara et al., 2018; Sung et al., 2014; Yang et al., 2013; Yuriar-Arredondo et al., 2018), protective clothing (Sundarrajan & Ramakrishna, 2007), wound dressing (Lee et al., 2014; Unnithan et al., 2014) and catalyst (Fang et al., 2011; Hu et al., 2014; Likhar et al., 2009; Yang et al., 2016). Sensing material (Ding et al., 2004; Manesh et al., 2007; Pinto et al., 2008) is one of the nanofibers applications due to its highly porous structure and the large surface-to-volume ratio enhancing sensitivity and rapid response rate (Cho et al., 2011; Khattab et al., 2016; Kumar et al., 2020; Wu et al., 2017; Zhi et al., 2012).

2.2 Conducting polymers

Conductive polymers (CPs) are organic materials with unique electrical and optical properties similar to inorganic semiconductors and metals (Nezakati et al., 2018). CPs are used in various applications such as supercapacitor, nanocoating, catalysis, biomedical including the sensors showed in Figure 2.3 (K & Rout, 2021). In sensors application, CPs are rapidly developed and have high potential in chemical gas sensors because the conductivity of CPs can change when exposed to oxidative or reductive gas molecules at room temperature (Ibanez et al., 2018; Wu, 2019). In general, CPs such as polyacetylene (PA), polyaniline (PANI), polypyrrole (PPy), polythiophene (PT), poly(3,4-ethylenedioxythiophene) (PEDOT), poly(phenylene vinylene) (PPV) and their derivatives with typical π -conjugated structures show p-type conductive behaviors. When they interact with gas molecules, they behave either as an electron donor or an electron acceptor. Therefore, if the concentration of gas molecules increases or decrease, it results in a change of their conductivity or resistivity (Yan et al., 2020).

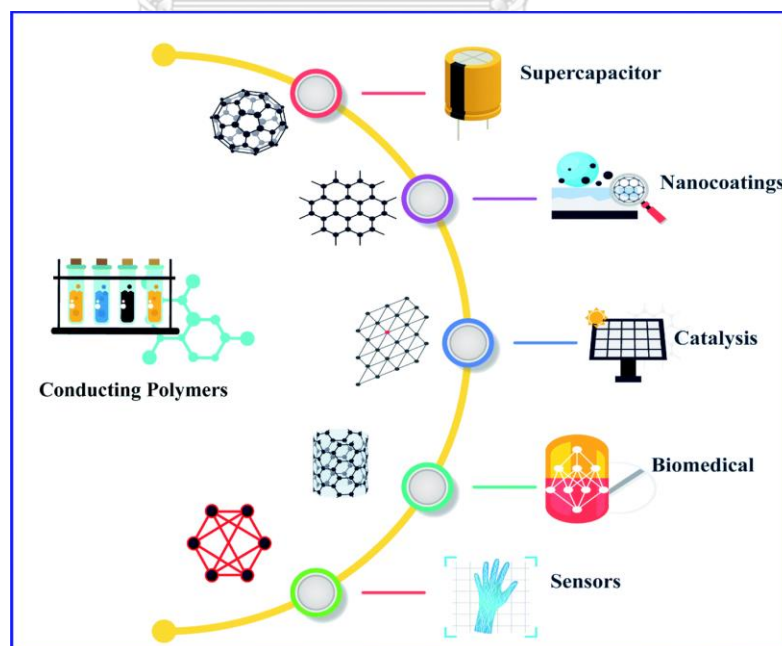


Figure 2.3 Schematic illustration of applications of conducting polymers and their composites.

2.3 CPs-metal oxide composite for gas sensing

CPs-based sensors are widely used for gas detection due to their very good electrochemical properties. The advantages of CPs include low cost, long-term stability, and easy synthesis. However, there are disadvantages such as low sensitivity, slow response and lack of recovery process, poor thermal stability, and insufficient selectivity (Yan et al., 2020). By contrast, metal oxide semiconducting sensors have attracted enormous interest because of their cost efficiency, stability, and sensing of most toxic gases (Ju et al., 2014; Sui et al., 2015). However, metal oxide semiconducting sensors have a lack of flexibility and selectivity. They have to be operated at high temperatures, and they are hazards, and short lifetimes (Ju et al., 2015). Consequently, a minimizing disadvantage is to combine CPs with a metal oxide, which achieves the excellent detection performance of the novel sensing material over its constituent components. CPs-metal oxide composites act as p-n junction semiconductors in order to overcome the problems related to a high rate of electron-hole recombination, thermal decomposition and improve sensitivity for gas detection (Tran et al., 2021).

2.4 Mechanism of tin dioxide nanofibers@polyaniline nanocomposite (SnO₂ NFs@PANI) to NH₃

The SnO₂ NFs@PANI sensor is a p-n junction at the interface between PANI and SnO₂ nanofibers. Typically, PANI is considered as p-type semiconductor that exhibits holes conductivity. It can be interpreted as the deprotonation/ protonation process via adsorption/desorption of NH₃ gas. As NH₃ gas is presented on PANI, the lone pair electron of NH₃ gas adsorbed on coordination bonding with the proton resulting in deprotonation of nitrogen atoms on PANI (Figure 1.2). As a result of the deprotonation, the charge carriers disappears and hence the electrical conductivity decreases. This causes the transformation of PANI from emeraldine salt (ES) to emeraldine base (EB), which led to the increase of resistance (Jia et al., 2020; C. Liu et al., 2018; Mikhaylov et al., 2015; Nicolas-Debarnot & Poncin-Epaillard, 2003; Tanguy et al., 2018). In contrast, after the sensor was exposed to air, PANI transforms back to ES again, which causes the resistance of PANI decreased. SnO₂ nanofibers acts as a n-type semiconductor which electron is the majority carrier. At the interface, the electrons of SnO₂ nanofibers recombine with holes in PANI until the p-n junction reaches the equilibrium state. The depletion region is then formed at the interface between the p-type PANI and n-type SnO₂ nanofibers (Ai et al., 2006; Awang, 2014; Bhowmick et al., 2020; Tai et al., 2007). When ammonia gas was introduced, NH₃ molecules are adsorbed on the surface of the sensor, based on SnO₂ NFs@ PANI nanocomposite withdrawal of protons from PANI, which leads to a decrease of holes concentration in PANI and the depletion layer at the interface. Thus, the resistance of the SnO₂ NFs@ PANI sensor further increased. Therefore, the formation of the p-n junction structure and the nanostructure of the SnO₂ NFs@ PANI sensor can improve the NH₃ gas sensing performance.

2.5 Response, response time and recovery time

In general, NH_3 gas sensor analysis is measured in resistivity and popularly reported as a ratio of resistance (response) compared to time. So, response (S) is defined by the expression $(R_g - R_a)/R_a$, $(R_g - R_a)/R_a \times 100\%$ or R_g/R_a where R_a and R_g are the measured resistances of the sensor exposed to air and test gas, respectively. Response time (t_{res}) (s) is the time required for a sensor to reach 90% of the maximum response of the signal such as resistance upon exposure to test gas. Recovery time (t_{rec}) (s) is the time required for a sensor to reach 90% of the original baseline resistance upon removal of the test gas (Chiu & Tang, 2013). These parameters are showed in Figure 2.4. The t_{res} and t_{rec} indicate the absorption and desorption properties of the gas to be analyzed. A good sensor should have low t_{res} and t_{rec} .

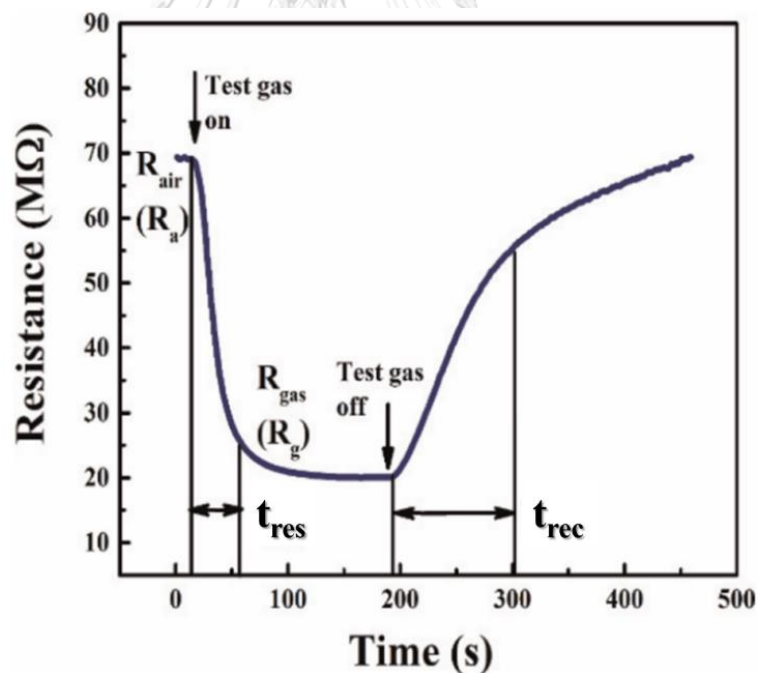


Figure 2.4 Resistance transient of an n-type gas sensor shows stable resistance in air (R_a), stable resistance in gas (R_g), response time (t_{res}), and recovery time (t_{rec}).

2.6 Properties of gas-sensing material

Sensing material is a very important part of the sensor. It is the part that indicates the effectiveness of the sensor. Required and undesired properties of sensing material are showed in the Table 2.1 (Feng et al., 2019; H. Liu et al., 2018; Mikołajczyk et al., 2016; Sanjeeda & Taiyaba, 2014; Wilson & Baietto, 2009).

Table 2.1 Required and undesired properties of gas-sensing material.

Required properties	Undesired properties
<ul style="list-style-type: none"> - Wide range of target gases - Long lifetime - Simple and portable - Fast response and recovery time (low t_{res} and t_{rec}) - Reversible gas adsorption - High conductance change - Diverse sensor coatings - Strong biomolecular interactions 	<ul style="list-style-type: none"> - Sensitive to environmental - High energy consumption - Susceptible to contaminants

2.7 NH₃ gas sensor

Up to date, several types of NH₃ gas sensors are developed. Common ammonia gas sensors are showed in the Table 2.2.

Table 2.2 Currently available NH₃ gas sensors with their properties.

Sensor	Range (ppm)	Response time	Operating temp. (°C)	Expected lifetime	Advantage	Weakness
NE4-NH ₃ 	0 – 100	< 90 s	-30 - 50	>2 years	<ul style="list-style-type: none"> - Long-term stability - Fast response 	<ul style="list-style-type: none"> - Store under 20°C - Sensor is blocked with water drops or other liquid
ZE03-NH ₃ 	0 – 100	No data	0 - 50	>1 year	<ul style="list-style-type: none"> - Long-term stability - Storage Environment (0 – 55°C) 	<ul style="list-style-type: none"> - Interference to various gas
MIX8415 	0 – 100	< 60	-20 - 50	1 year	<ul style="list-style-type: none"> - High selectivity & sensitivity 	-
AR8500 	0 – 100	<120	-10 - 40	2 years	<ul style="list-style-type: none"> - Long-term stability 	<ul style="list-style-type: none"> - Slow response
ATO-GAS-NH ₃ 	0 – 100	≤10	-20 - 50	1 year	<ul style="list-style-type: none"> - Fast response 	-

CHAPTER 3

EXPERIMENTAL

3.1 Instruments and apparatus

- 3.1.1 Hantek 365F PC USB Digital Multimeter, Hantek.eu., Czech
- 3.1.2 In-house gas detector
- 3.1.3 In-house screen-printed electrode template (Figure 3.1)
- 3.1.4 Scanning electron microscope/energy dispersive spectroscopy (SEM-EDS; JSM-IT100 InTouchScope, JEOL Ltd., Japan)
- 3.1.5 X-Ray Diffraction (XRD; 9kW SmartLab X-Ray diffractometer (CuK α /radiation, 40 kV, 30 mA) with a D/teX Ultra 250 detector, Rigaku Co., Japan)
- 3.1.6 Vacuum pump
- 3.1.7 Oven

3.2 Chemicals and materials

- 3.2.1 Tin(II) chloride dihydrate (SnCl $_2$ · 2H $_2$ O, purity 99 %), Sigma-Aldrich Co., USA
- 3.2.2 Tin oxide powder (SnO $_2$), Sigma-Aldrich Co., USA
- 3.2.3 Aniline (purity 98.5 %), Sigma-Aldrich Co., USA
- 3.2.4 Dimethylformamide (DMF), Sigma-Aldrich Co., USA
- 3.2.5 Ammonium peroxydisulphate (APS, purity 99 %), Sigma-Aldrich Co., USA
- 3.2.6 Polyacrylonitrile (PAN, MW = 150,000), Sigma-Aldrich Co., USA
- 3.2.7 Polyvinylpyrrolidone (PVP, MW = 1,000,000), Sigma-Aldrich Co., USA
- 3.2.7 Hydrochloric acid (HCl, 37%), Sigma-Aldrich Co., USA
- 3.2.8 Ethanol (CH $_3$ CH $_2$ OH) (95%), Sigma-Aldrich Co., USA
- 3.2.9 Acetone (C $_3$ H $_6$ O), Merck Co., Germany
- 3.2.10 Methanol (CH $_3$ OH), Merck Co., Germany
- 3.2.11 Toluene (C $_6$ H $_5$ CH $_3$), Merck Co., Germany

3.2.12 Formaldehyde (CH₂O), Quality Reagent Chemical Co., New Zealand

3.2.13 Conductive ink

- Carbon ink (Gwent Electronic Materials Ltd., UK.)

- Graphene ink (Sun Chemical Co., USA.)

3.2.14 Acrylic, Ekasilpbangkok Co., Thailand

3.2.15 Ceramic, obtained from a calcination of aluminum oxide (Al₂O₃) at 1050 °C.

3.2.12 Polyvinyl chloride sheet (PVC sheet)

3.2.13 Filter paper No.42

3.3 Preparation of SnO₂ nanofibers by electrospinning technique

A selected polymer (PAN or PVP) was dissolved in 5 mL DMF at 80 °C with a stirring for 2 hrs. A 10% SnCl₂·2H₂O was further added into the solution and stirred for 1 hr. The prepared solution was then loaded into a syringe which connected to a 0.7 mm diameter stainless-steel needle. The needle tip was set at 15 cm away from a rotating collector that was wrapped with aluminum foil. Electrospinning was carried out by applying 16 kV electric field across the needle and rotating collector while a 13 μL/min feeding rate was applied to the syringe (Figure 3.1). The obtained nanofibers were then calcinated at 600 °C in the air for 2 hrs to remove the organic constituents of polymer (PAN or PVP) and further crystalize SnO₂. Morphology of the composite nanofibers was characterized, and an energy scattering pattern was obtained using a scanning electron microscope/energy dispersive spectroscopy (SEM-EDS). The XRD patterns were obtained by a Rigaku 9 kW SmartLab X-Ray diffractometer (CuKα/radiation, 40 kV, 30 mA) with a D/teX Ultra 250 detector.

Noted here that the optimized process above came from variation studies of

- Polymer types: polyacrylonitrile (PAN) and polyvinylpyrrolidone (PVP)
- Percentage of polymer: 7% and 10% PAN, 7% PVP
- Percentage of SnCl₂ · 2H₂O: 10, 15, and 20%

- Electrospinning collector types: fixed and rotating collectors

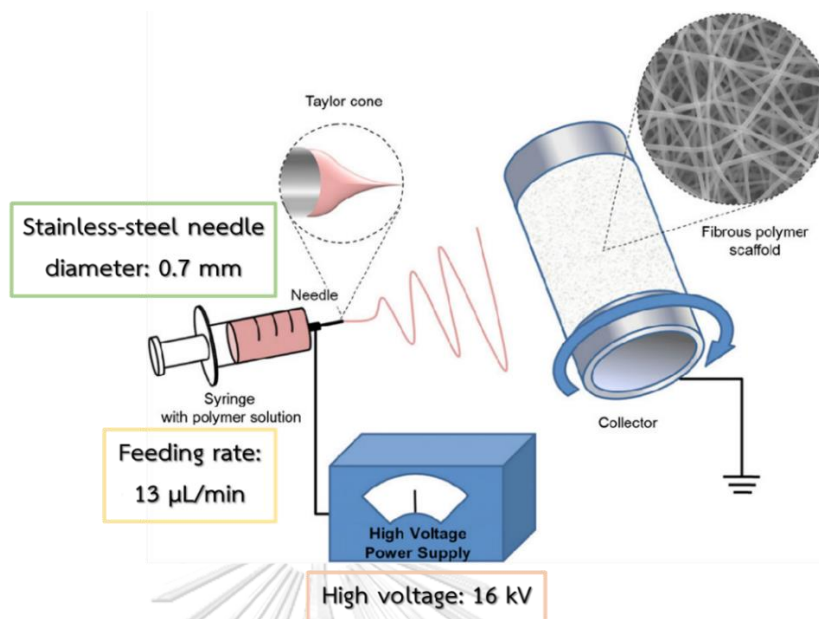


Figure 3.1 Scheme of electrospinning technique for preparation of SnO₂ NFs.

3.4 Synthesis of NH₃-sensing materials

3.4.1 Pure polyaniline (PANI)

Solution A was prepared by sonicating 46 μL of 10.79 M aniline monomer in 15 mL 1 M HCl for 30 mins. Solution B was prepared by adding 0.114 g of ammonium peroxydisulphate (APS) into 15 mL of 1 M HCl and stirred for 30 mins. Then, solution A and solution B were mixed and stirred for 30 mins. An *in-situ* chemical polymerization took place at room temperature within 1 hr. Finally, the pure PANI was obtained after being filtered and washed with 95% ethanol to eliminate unreacted aniline monomer from the PANI precipitate. After that, the PANI precipitates were washed with 1 M HCl to convert to emeraldine salt (ES). Lastly, the precipitate was collected and dried in air for 24 hrs. Morphology of the composite was characterized and energy scattering pattern was obtained using a scanning electron microscope/energy dispersive spectroscopy (SEM-EDS). The XRD patterns was obtained by a Rigaku 9 kW SmartLab X-Ray diffractometer (CuKα/radiation, 40 kV, 30 mA) with a D/teX Ultra 250 detector.

3.4.2 SnO₂/PANI

The SnO₂/PANI was prepared by the same procedure as written in 3.4.1 except the composition in solution A. To prepare SnO₂/PANI, solution A was prepared by sonicating 1 mg SnO₂ powder in 15 mL of 1 M HCl for 10 mins. Then, 46 μL of 10.79 M aniline monomer was added and continue sonicated for another 30 mins.

3.4.3 SnO₂ NFs@PANI

The SnO₂ NFs@PANI was prepared by the same procedure as written in 3.4.2 except the composition in solution A. To prepare SnO₂ NFs@PANI nanocomposite, SnO₂ nanofibers synthesized in 3.3 was added, instead of SnO₂ powder. Then, modify the SnO₂ NFs@PANI on screen-printed graphene electrode (SPGE) substrate.

Noted here that the optimized process above came from variation studies of

- Weight of SnO₂ NFs in PANI: 1, 2, 4, and 7 mg
- Time of SnO₂ NFs@PANI synthesis process: 0.5, 1, 2, 4, and 6 hr.
- Filtration method for SnO₂ NFs@PANI synthesis process result diagnosis: vacuum pump and gravity.

3.5 Fabrication of screen-printed electrode

Fabrication process of screen-printed electrodes (SPEs) begins by rinsing the SPE template (Figure 3.2) with acetone, and then let it dry. Carbon ink or graphene ink was screen-printed on the PVC sheet as a working electrode. After that, the electrodes were baked in oven at 55 °C for 1 hr.

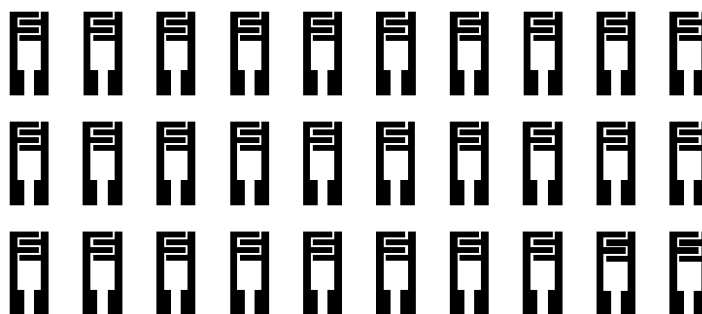


Figure 3.2 Screen-printed electrode for NH₃ sensors

3.6 Sensor fabrication

To fabricate a sensor, each of NH_3 sensing materials; pure PANI, SnO_2/PANI or SnO_2 NFs@PANI was weighted and dispersed in 1 mL DMF. Then, 60 μL of the mixture was drop-cast on different substrates; acrylic, ceramic, screen-printed carbon electrode (SPCE) or screen-printed graphene electrode (SPGE), and dried in oven at 55 $^\circ\text{C}$ for 20 mins.

Variable parameters that were examined in this process were:

- Types of sensing material
- Types of substrates
- Numbers of drop-casting layer
- Concentration of SnO_2 NFs@PANI in DMF solution

3.6.1 Types of sensing material

A 1 mg of pure PANI, SnO_2/PANI and SnO_2 NFs@PANI were weighted out and prepared by the process written above. Each of these sensing materials was drop-cast (10 layers) on a screen-print carbon electrode (SPCE). Their responses to 0.6 ppm ammonia gas were recorded and compared.

3.6.2 Types of substrates

A 1 mg of SnO_2 NFs@PANI were weighted out and prepared by the process written in 3.6. It was, then, drop-cast (10 layers) on four different substrates: acrylic, ceramic, SPCE, and SPGE. Their response to 0.6 ppm ammonia gas were recorded and compared.

3.6.3 Numbers of drop-casting layer

A 2 mg of SnO_2 NFs@PANI were weighted out and prepared by the process written in 3.6. It was, then, drop-cast on screen-print graphene electrode (SPGE) using 2, 4, 6, 8 and 10 layer Their response to 10 ppm ammonia gas were recorded and compared.

3.6.4 Concentration of SnO₂ NFs@PANI in DMF solution

The 1, 2, 5, and 7 mg of SnO₂ NFs@PANI in DMF solution were separately modified on screen-print graphene electrode (SPGE). Their response to 10 ppm ammonia gas were recorded and compared.

3.7 Performance of NH₃ sensor

In the gas measurement, the fabricated sensor was placed the in-house gas detector (Figure 3.3) and was connected to the digital multimeter. Resistances were continuously recorded, at room temperature (30 ± 5 °C) when the gas chamber was filled with a desired concentration of NH₃ and when the NH₃ was flushed out by air. The NH₃ concentration was calculated based on the content of the injected liquid. The concentration (C) of injected NH₃ in the container was calculated by the following equation 3.1 (W. Wang et al., 2020; Xianfeng Wang et al., 2012):

$$C = (22.4\rho TV_s/273MV) \times 1000 \quad (\text{equation 3.1})$$

Where C is the concentration of gaseous ammonia (ppm), ρ is the density of liquid ammonia (g/mL), T is the testing temperature (K), V_s is the volume of liquid ammonia (μ L), M is the molecular weight of ammonia (g/mol), and V is the volume of the chamber (L).

จุฬาลงกรณ์มหาวิทยาลัย
CHULALONGKORN UNIVERSITY

The response (S) of the fabricated sensor was defined by equation 3.2 (Li, Wang, et al., 2018; Pang et al., 2014):

$$S = (R_g - R_a)/R_a \quad (\text{equation 3.2})$$

The R_g represents resistance of the sensor in NH₃ gas and R_a is a resistance of the sensor in air. The response and recovery times are defined as the time required for the sensor to achieve 90% of stable resistance, when the fabricated sensor was exposed to the NH₃ gas and air, respectively (Shalan et al., 2019), as showed in Figure 3.4.

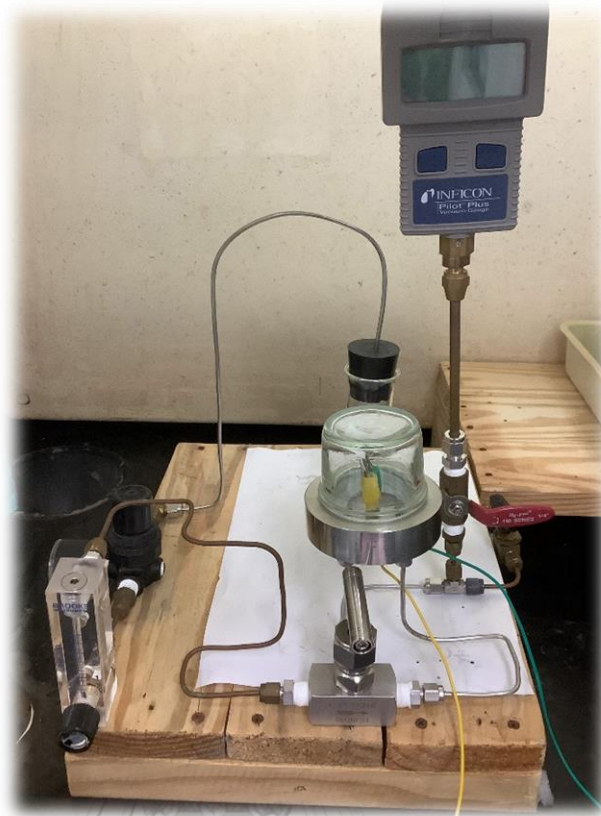


Figure 3.3 In-house gas detector.

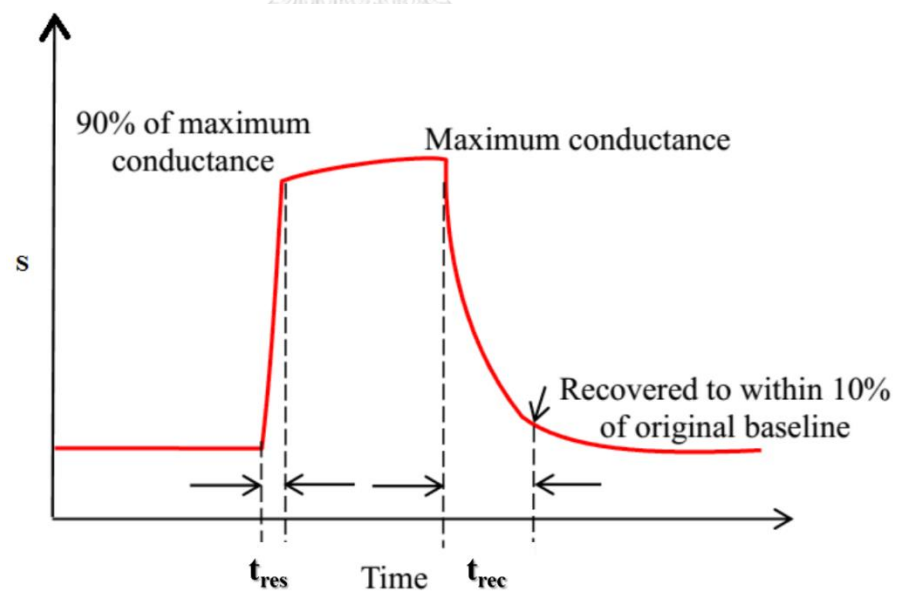


Figure 3.4 The response and recovery times.

3.7.1 Linear range and limit of detection

The sensor performance was tested with many NH_3 concentrations (0.4 - 100 ppm) at room temperature (30 ± 5 °C). The measurements at each NH_3 concentration were repeated three times. The measured responses were plotted against the ammonia concentration and standard deviation (SD) was calculated.

The lowest detectable NH_3 concentration (0.4 ppm NH_3 gas) was repeatedly measured for 20 times. The limit of detection (LOD) was calculated using $3\text{SD}/\text{Slope}$ method, as showed in equation 3.3:

$$\text{LOD} = 3\text{SD}/\text{Slope} \quad (\text{equation 3.3})$$

3.7.2 Selectivity

The 10 ppm of selected gas; acetone: $\text{C}_3\text{H}_6\text{O}$, ethanol: $\text{C}_2\text{H}_6\text{O}$, formaldehyde: CH_2O , methanol: CH_3OH and toluene: $\text{C}_6\text{H}_5\text{CH}_3$ was place in the in-house gas detector and measured by our fabricating sensor for three time. Their responses were compared with the 10 ppm NH_3 gas.

3.7.3 Repeatability

The 10 ppm NH_3 and air were place into the in-house gas detector at the other time. Ten measurement cycles were performed on one sensor. The continuous response was recorded, and the standard deviation (SD) was calculated.

3.7.4 Reproducibility

Five SnO_2 NFs@PANI sensors were tested with 10 ppm NH_3 gas. The reproducibility response was reported, and the percentage of relative standard deviation (%RSD) was calculated.

3.7.5 Long-term stability

A SnO_2 NFs@PANI sensor was exposed to 10 ppm NH_3 for about 2 months. Every 7 days, the response was recorded, and the standard deviation (SD) and the percentage of stability were calculated.

3.7.6 Application of the SnO₂ NFs@PANI sensor in fish freshness evaluation

In favor of the fabricated SnO₂ NFs@PANI sensor application, a piece of fresh fish was cut into pieces of 5 g, and separately stored them in the test chamber at room temperature and in freezer (or refrigerator) at 4 °C. The sensor was used to determine the content of NH₃ releasing from the fish filet every 1 hr compared to the sniffing and color changing observation.



CHAPTER 4

RESULTS & DISCUSSION

Tin dioxide nanofibers@polyaniline nanocomposite (SnO_2 NFs@PANI) was synthesized and examined as an ammonia gas sensor. The composition of this sensor can be divided into three main procedures: electrospinning techniques, *in-situ* polymerization, and sensor fabrication.





4.1 Preparation of SnO_2 nanofibers by electrospinning

SnO_2 nanofibers were prepared by the electrospinning technique. Briefly, polymer (PAN, PVP) was dissolved in 5 mL DMF at 80 °C with a stirring for 2 hrs, followed by the addition of $\text{SnCl}_2 \cdot 2\text{H}_2\text{O}$ into the solution and stirred for 1 hr. The prepared solution was then loaded into the syringe for the electrospinning technique. The obtained nanofibers were then calcinated at 600 °C in the air for 2 hrs. Noted here that the optimized process above came from variation studies of type and percentage of polymer, percentage of $\text{SnCl}_2 \cdot 2\text{H}_2\text{O}$, and types of collectors. Morphology of the composite nanofibers was, then, characterized by SEM-EDS and XRD.

4.1.1 Type of polymer and its percentage

Two types of polymers: polyacrylonitrile (PAN) and polyvinylpyrrolidone (PVP), and their percentages: 7 %w/v and 10 %w/v were investigated for nanofibers formation through the electrospinning technique. The result comparison showed in the Table 4.1

Table 4.1 Types and percentages of polymer for nanofibers formation by electrospinning.

Types and percentages of polymer	Photographs of nanofibers	
	Before calcined at 600 °C	After calcined at 600 °C
7 %w/v PVP + 10 %w/v SnCl ₂ · 2H ₂ O		
7 %w/v PAN + 10 %w/v SnCl ₂ · 2H ₂ O		
10 %w/v PAN + 10 %w/v SnCl ₂ · 2H ₂ O	Highly viscous (could not be processed by electrospinning)	-

A 7 %w/v of each polymer mixed with a fixed 10 %w/v SnCl₂ · 2H₂O was spun and calcined. The appearances of the obtained nanofibers, before and after the calcination, were showed in Table 4.1. Before the calcination, both spun fibers appeared as white sheets. During the calcination at 600 °C for 3 hrs hydroxides were converted to oxides, polymer decomposed, and crystals of SnO₂ were form (Liu et al., 2021). After the calcination, SnO₂ nanofibers sheet obtained from the 7 %w/v PVP solution broke down and turned into powder. Fortunately, a different result was observed in the 7 %w/v PAN solution. A white and fragile SnO₂ nanofibers sheet

remained in a piece. However, a higher percentage of PAN (10 %w/v) could not process with the electrospinning due to the excessive viscosity of the solution.

Therefore, the 7 %w/v PAN seems to be the most appropriate base polymer for the SnO₂ nanofibers formation via electrospinning.

4.1.2 Percentage of SnCl₂ · 2H₂O in the nanofibers

The richer SnO₂ nanoparticle, the better fibers that we prefer. Thus, different percentages of SnCl₂ · 2H₂O; 10 %w/v, 15 %w/v, and 20 %w/v, were added into 7%w/v PAN and the resulted nanofibers were investigated.

Table 4.2 Percentages of SnCl₂ · 2H₂O in the nanofiber formation by electrospinning.





Percentages of SnCl ₂ · 2H ₂ O	Photographs of nanofibers	
	Before calcined at 600 °C	After calcined at 600 °C
10 %w/v SnCl ₂ · 2H ₂ O		
15 %w/v SnCl ₂ · 2H ₂ O		
20 %w/v SnCl ₂ · 2H ₂ O	Not dissolvable in 7 %w/v PAN	-

Table 4.2. shows the result of 7 %w/v PAN mixed with various percentages of SnCl₂ · 2H₂O, before and after the calcination. By adding 10 %w/v SnCl₂ · 2H₂O, the fibers appeared white both before and after the calcination. However,

when the $\text{SnCl}_2 \cdot 2\text{H}_2\text{O}$ concentration increased to 15 %w/v the fibers turned grey after the calcination, there is a possibility that SnO_2 crystals can trap the carbon molecule, resulting in gray nanofibers. Attempt on adding a higher percentage of $\text{SnCl}_2 \cdot 2\text{H}_2\text{O}$ was ended at 20 %w/v because not all the $\text{SnCl}_2 \cdot 2\text{H}_2\text{O}$ could be dissolved in 5 mL of 7 %w/v PAN.

Thus, 10 % w/v $\text{SnCl}_2 \cdot 2\text{H}_2\text{O}$ was the highest percentage that gave the most desirable nanofibers result and was suitable for further analysis.

4.1.3 Types of collectors in electrospinning

In the formation process of nanofibers via electrospinning, two types of collectors, a fixed sheet, and a rotating collector, were studied.

Table 4.3 Types of collectors in electrospinning for nanofibers formation.

A 10 %w/v $\text{SnCl}_2 \cdot 2\text{H}_2\text{O}$ mixed with 7 %w/v PAN was used in this test.

Types of collectors	Photographs of nanofibers	
	Before Calcined at 600 °C	After Calcined at 600 °C
Fixed sheet collector		No result
Rotating collector		

Pictures of the nanofibers formed on each collector were showed in Table 4.3. Prior to the calcination, the nanofibers formed on a fixed sheet showed disorganized and uneven surface while one formed on a rotating collector showed close arrangement, neat and smooth surface. After calcination, the nanofibers obtained from the rotating collector appeared as white nanofibers sheet.

Thus, the rotating collector is a better collector than a fixed sheet collector, in this case.

4.1.4 Characterization of SnO₂ nanofibers

Figure 4.1 A and B shows differences in the morphology of PAN/SnCl₂ nanofibers before calcination and SnO₂ nanofibers (SnO₂ NFs) after the 600 °C calcination . From SEM images, the diameter of as-synthesized PAN/SnCl₂ (Figure 4.1A) was higher than SnO₂ nanofibers (Figure 4.1B, around 1 μm), which may due to the combining process of SnCl₂ in the PAN nanofibers (Wang et al., 2011). As SnCl₂ molecule are much smaller than PAN polymer, they could reach the outer boundary layer of the fibers easily. As a result, SnCl₂ distributed on the surface while PAN located in the center line of the fibers. After calcination, PAN decomposed and porous SnO₂ hollow nanofibers were formed. The EDS mapping images (Figure 4.2) confirm the existence of Sn, C, and O without impurities in the PAN/SnCl₂ (before calcination) and SnO₂ NFs (after calcination). Figure 4.2A shows XRD pattern of PAN/SnCl₂ which indicate no present of SnO₂. Figure 4.2B shows XRD pattern of the SnO₂ NFs. The prominent peaks of SnO₂ NFs are corresponding to 26.58° (1 1 0), 33.85° (1 0 1), and 51.80° (2 1 1) crystal lattice planes. Therefore, the XRD pattern of the SnO₂ NFs prepared by electrospinning was in good agreement with those of X-ray standard data and the sharp diffraction peaks (ICSD Code: 183984) suggest that annealing at 600 °C for 3 hrs. was adequate to SnO₂ NFs formation.

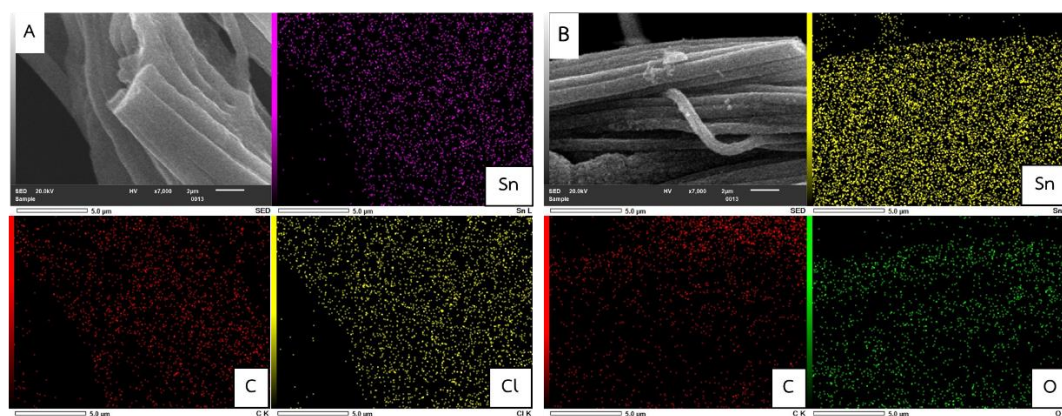


Figure 4.1 SEM images and EDS mapping of (A) PAN/SnCl₂ nanofibers and (B) SnO₂ nanofibers.

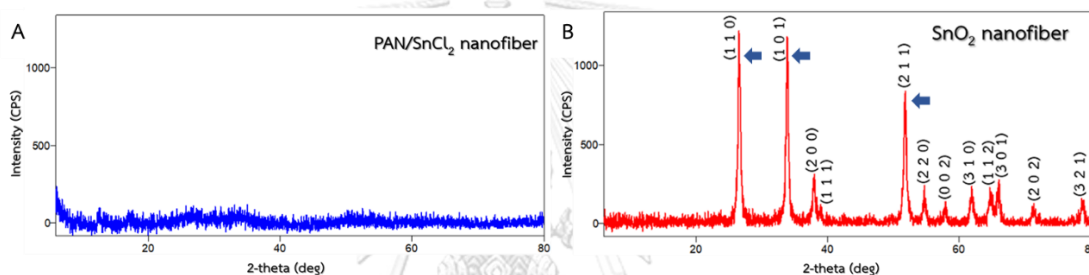


Figure 4.2 XRD patterns of (A) PAN/SnCl₂ nanofibers and (B) SnO₂ nanofibers.

4.2 *In-situ* polymerization of SnO₂ NFs in PANI

After the SnO₂ NFs was formed it was doped into polyaniline (PANI) by an *in-situ* polymerization process at room temperature. In procedure, the SnO₂ NFs was added to an aniline monomer solution followed by ammonium peroxydisulphate (APS). The *in-situ* polymerization process begins. To reach completeness of the polymerization, at least 6 hrs. was suggested (Abu-Thabit, 2016; Beygisangchin et al., 2021). This process was time consuming. Therefore, in order to shorten and optimize the *in-situ* polymerization procedures studies variation include weight of SnO₂ NFs, *in-situ* polymerization time and types of filters were necessary. Morphology of the obtained SnO₂ NFs@PANI composite was characterized by SEM-EDS and XRD.

4.2.1 Weight of SnO₂ NFs in PANI

Different weight of SnO₂ NFs in which prepared by the procedure as written in 3.4.3; 1, 2, 4, and 7 mg, were used to prepare the SnO₂ NFs@PANI composite. Figure 4.3 illustrates 10 ppm ammonia gas responses on 1, 2, 4, and 7 mg SnO₂ NFs composited with PANI that was, then, cast on screen-print graphene electrode (SPGE). A higher response was observed when the SnO₂ NFs was increased from 1 mg to 2 mg. However, a decrease in response was found when the amount of SnO₂ NFs increased from 2 mg to 7 mg. This is due to a large amount of SnO₂ NFs which is a semiconductor that affects the high resistance of the sensor in air (R_a) before gas detection, resulting in a lower signal response ratio.

As the 2 mg SnO₂ NFs in composited with PANI gave the highest response to the NH₃ gas as shown in Table 4.4. The 2 mg SnO₂ NFs was, then, chosen for the *in-situ* polymerization of SnO₂ NFs@PANI.

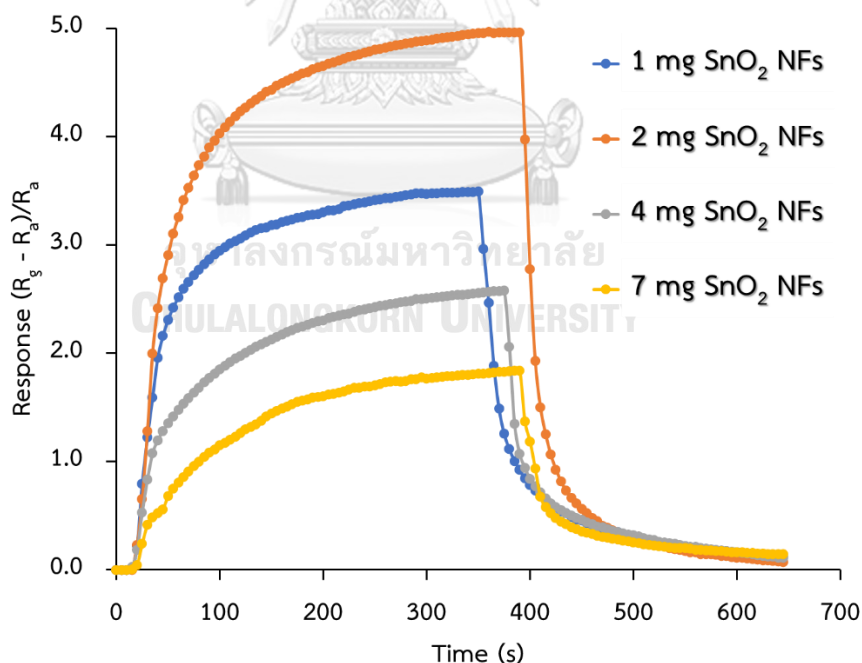


Figure 4.3 10 ppm NH₃ gas responses on 1, 2, 4, and 7 mg SnO₂ NFs that was composited with PANI and was, then, cast on SPGE.

Table 4.4 Responses of the SnO₂ NFs@PANI composites, prepared from different weight of SnO₂ NFs to 10 ppm NH₃.

Weight of SnO ₂ NFs	Response				SD
	st 1	nd 2	rd 3	Average	
1 mg	3.80	3.43	3.20	3.48	0.30
2 mg	5.00	4.48	5.19	4.89	0.37
4 mg	2.53	2.58	2.42	2.51	0.08
7 mg	2.33	1.59	1.41	1.78	0.49

4.2.2 Time for *in-situ* polymerization

Different polymerize times: 0.5, 1, 2, 4, and 6 hrs were tested. Figure 4.4 illustrates 10 ppm ammonia gas responses on 2 mg SnO₂ NFs composited with PANI for 0.5, 1, 2, 4, and 6 hrs. Higher response was observed when the polymerize time was increased from 30 mins to 1 hr. This is due to the ammonium peroxydisulphate (APS) and aniline reacting completely, forming a long chain of PANI which has good electrical conductivity (Mazzeu et al., 2018). However, a decrease in response was found when the polymerize time was increased from 1 hr to 2 hrs. This can be explained by the oxidative degradation of the polymer, because of the high concentration of APS, which promoted the formation of oligomers can be a large amount of water-soluble material and non-conductive (Chen et al., 2018). When the polymerize time was increased from 2 hrs to 6 hrs, increasing response indicates a stabilization of PANI synthesis (Mazzeu et al., 2018). Therefore, we found that the composite that was polymerized for 1 hr gave a response to the 10 ppm NH₃ as good as the one that was polymerized for 6 hrs as shown in Table 4.5. When calculated by Student's t-test (Table 4.6), it shows that the *t* value is less than $t(\alpha = 0.01)$, indicating that the polymerize times of 1 hr and 6 hrs were not significantly different.

Therefore, 1 hr polymerize time seem to be enough and was, then, chosen for the further polymerization.

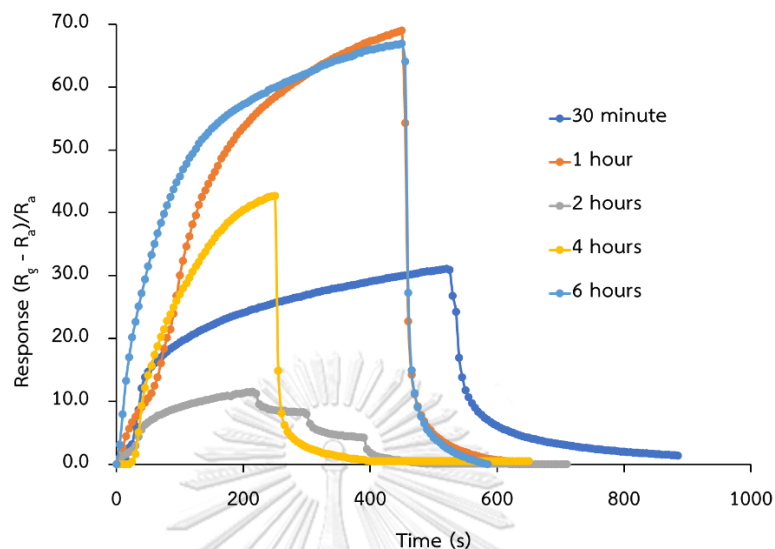


Figure 4.4 10 ppm NH_3 gas responses on 0.5, 1, 2, 4, and 6 hrs. polymerize time for 2 mg SnO_2 NFs composited with PANI and was, then, cast on SPGE.

Table 4.5 Response of polymerize time to prepare the SnO_2 NFs@PANI composite.

Polymerize time	Response				SD
	st 1	nd 2	rd 3	Average	
30 minutes	29.35	33.01	30.94	31.10	1.50
1 hour	71.10	69.00	66.90	69.00	1.71
2 hours	11.10	11.60	12.00	11.57	0.37
4 hours	42.60	45.30	49.80	45.90	2.97
6 hours	66.50	65.80	68.50	66.93	1.40

Table 4.6 t-test value of polymerize time to prepare the SnO₂ NFs@PANI composite.

	1 hr.	6 hrs.
Mean	69.00	66.93
SD	2.10	1.40
SD ²	4.41	1.96
S _c ²	3.19	
SE _D	1.46	
t _{test}	1.42	
df	4	
t(α = 0.01)	4.604	

4.2.3 Filtration method for SnO₂ NFs@PANI synthesis process result diagnosis: vacuum pump and gravity.

The filtration method is an important part of obtaining the precipitate of SnO₂ NFs@PANI. Therefore, the filtration method must be studied to shorten the time in the synthesis process of the sensing material. Figure 4.5 shows 10 ppm ammonia gas responses on SnO₂ NFs@PANI composite that was filtration method by a vacuum pump and gravity under the same type of paper filter. A similar response was observed was showed in Table 4.7. This indicates that both types of filters didn't affect the polymerizing product. The benefit of the capability to use a vacuum pump instead of gravity, was not only reducing the solid waste but also accelerating the polymerizing process. As it took about 360 min filtration when the gravity was used and 10 min filtration with the vacuum pump. When calculated by Student's t-test (Table 4.8), it shows that the *t* value is less than $t_{(\alpha = 0.01)}$, indicating that the vacuum pump and gravity were not significantly different.

Therefore, the vacuum pump was chosen as it saved the experimental time.

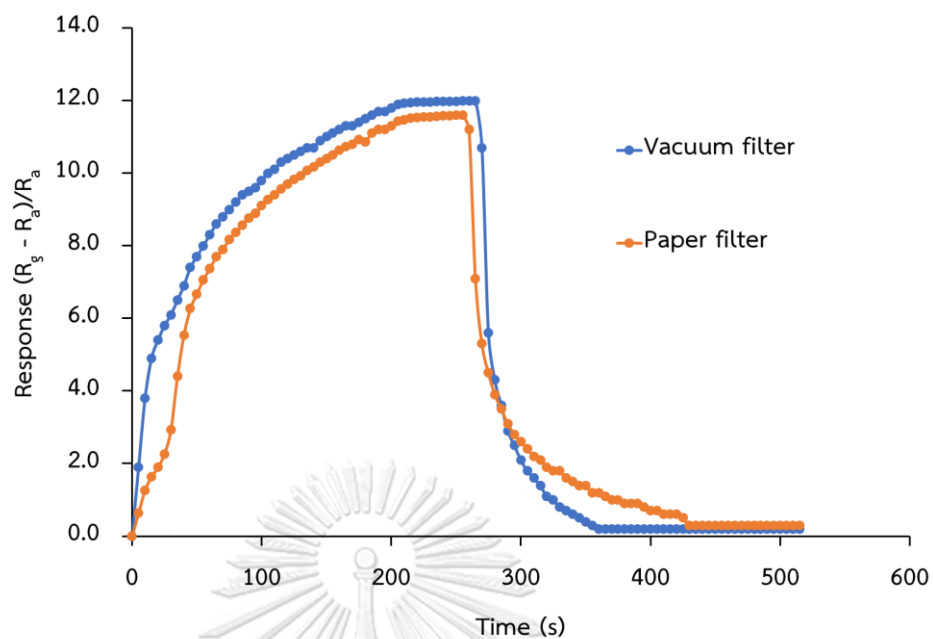


Figure 4.5 10 ppm NH_3 gas responses on vacuum pump (blue) and gravity (orange) for SnO_2 NFs@PANI composite.

Table 4.7 Response of filtration method of filters used at the end of SnO_2 NFs@PANI polymerization.

Filtration method	Response			Average	SD
	1 st	2 nd	3 rd		
Vacuum pump	11.99	11.59	13.30	12.30	0.90
Gravity	11.59	11.99	12.29	11.96	0.35

Table 4.8 t-test value of filtration method of filters used at the end of SnO₂ NFs@PANI polymerization.

	Vacuum filter	Paper filter
Mean	12.30	11.96
SD	0.90	0.35
SD ²	0.80	0.12
S _c ²	0.46	
SE _D	0.56	
t _{test}	0.61	
df	4	
t(α = 0.01)	4.604	

4.2.4 Characterization of SnO₂ NFs@PANI

After the polymerization, SEM image in Figure 4.6 shows well maintained fibrous network structure of PANI containing infiltrated SnO₂ NFs. High porosity and large surface area of SnO₂ NFs@PANI could be useful for improving the performance of NH₃ gas sensors. The EDS mapping images confirm existence of Sn, C, and O without impurities in the SnO₂ NFs@PANI. Figure 4.7 shows XRD spectrum of the PANI, SnO₂ NFs, and SnO₂ NFs@PANI. The pattern in Figure 4.7A reveals the characteristic peaks of PANI at 24.40° (1 0 0) and 25.60° (1 1 0). The prominent peaks of SnO₂ NFs in Figure 4.7B corresponding to 26.58° (1 1 0), 33.85° (1 0 1), and 51.80° (2 1 1). The XRD spectrum of SnO₂ NFs@PANI, Figure 4.7C, revealed the coexistence of PANI at 25.60° (1 1 0) and SnO₂ NFs components confirming the successful synthesise of SnO₂ NFs@PANI by the polymerization.

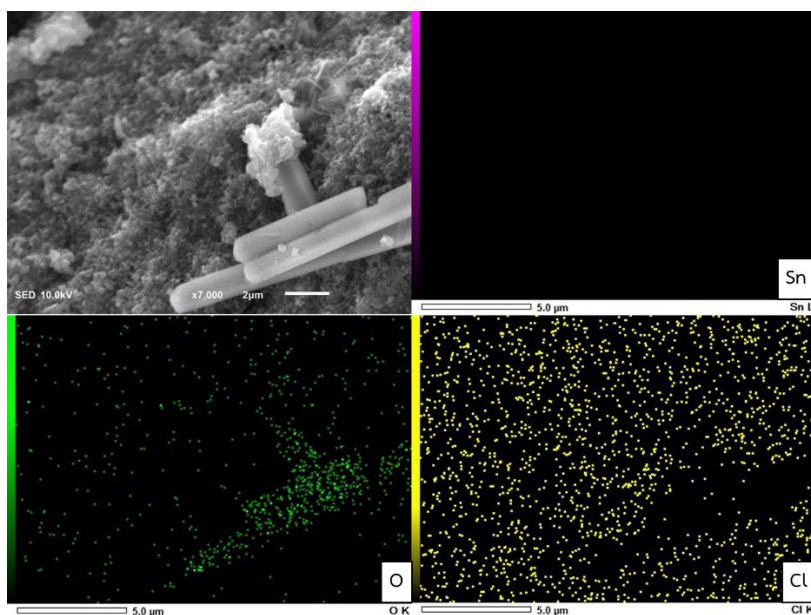


Figure 4.6 SEM images and EDS mapping of SnO₂ NFs@PANI

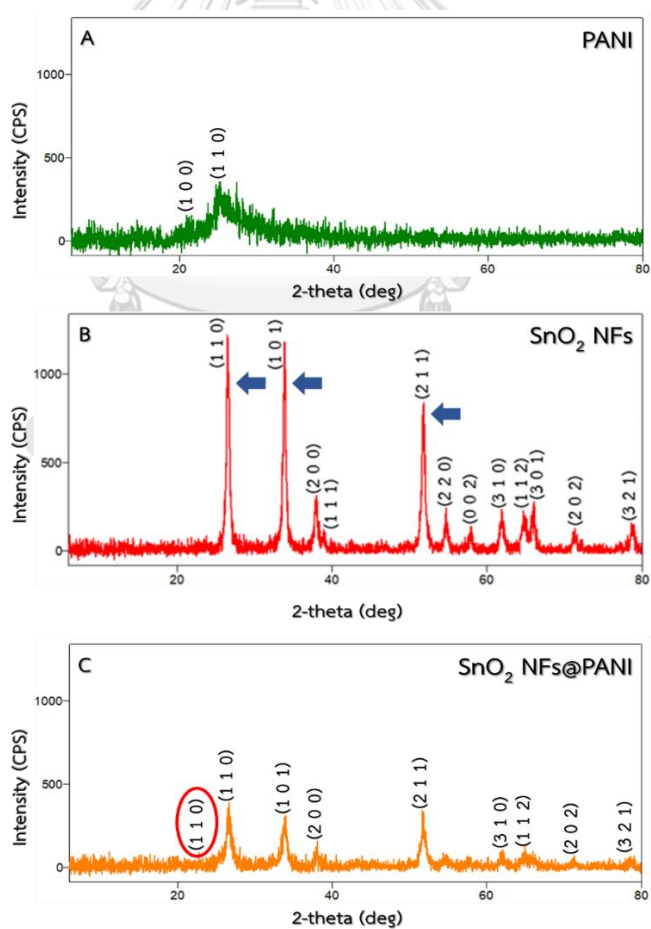


Figure 4.7 XRD patterns of (A) PANI, (B) SnO₂ NFs and (C) SnO₂ NFs@PANI.

4.3 Sensor fabrication

Fabrication of NH_3 sensors was done by dispersing a sensing material in 1 mL DMF and drop-casting it on a substrate at room temperature. To obtain the optimized conditions of the process, variation studies of types of sensing material, types of substrates, numbers of drop-casting layers, and concentration of sensing material in the DMF solution were investigated.

4.3.1 Types of sensing material and their response-recovery times

Three types of sensing material: pure PANI, SnO_2/PANI , and SnO_2 NFs@PANI were cast on SPCE. In this test, 0.6 ppm NH_3 gas was examined its obtained response and recovery times indicate the adsorption and desorption ability to the target gas measured by 90% of the maximum response upon exposure to test gas and 90% of the original baseline upon removal of the test gas, respectively (Kumar et al., 2020).

At room temperature, the NH_3 gas sensors made of PANI, SnO_2/PANI or SnO_2 NFs@PANI cast on SPCE substrate were compared (Figure 4.8). The responses for 0.6 ppm NH_3 were 0.29, 1.01, and 1.29 on the PANI, SnO_2/PANI , and SnO_2 NFs@PANI sensors, respectively. Among the three sensors, SnO_2 NFs@PANI gave the highest response as shown in Table 4.9 and fastest response (87 s) to NH_3 gas as well as the fastest recovery time (160 s) when compared to the PANI and SnO_2/PANI sensors. This is due to a high surface area of SnO_2 NFs@PANI when compared to the PANI and SnO_2/PANI sensing material. Compared to other studies (Table 2.2), the SnO_2 NFs@PANI sensor is usable due to its fast response.

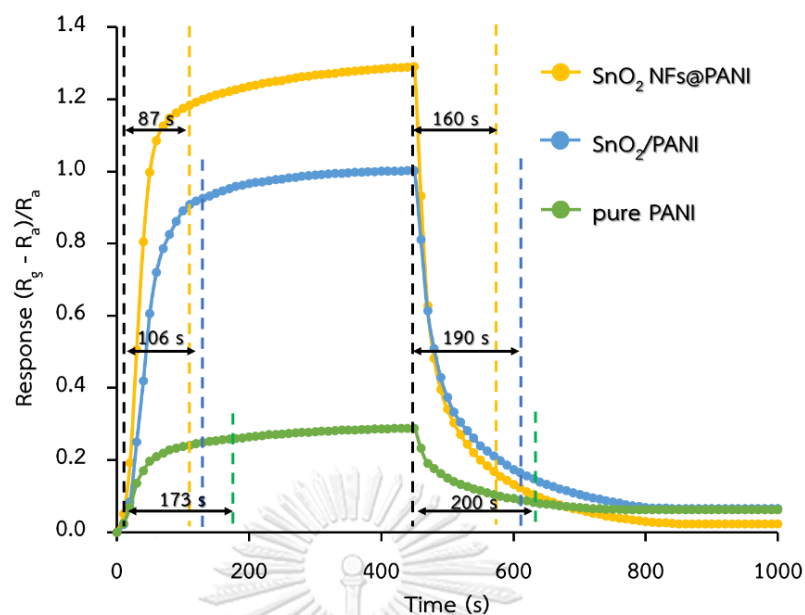


Figure 4.8 Responses, response times, and recovery times of 0.6 ppm NH_3 measured by pure PANI (green line), SnO_2/PANI (blue line), and SnO_2 NFs/PANI (yellow line) sensing materials cast on SPCE.

Table 4.9 Response of types of sensing material.

Types of sensing material	Response				SD
	1 st	2 nd	3 rd	Average	
pure PANI	0.29	0.28	0.30	0.29	0.01
SnO_2/PANI	1.01	1.00	1.00	1.01	0.01
SnO_2 NFs/PANI	1.28	1.30	1.29	1.29	0.01

4.3.2 Types of substrates

A 1 mg of SnO₂ NFs@PANI sensing material was cast on four types of substrates: SPGE, SPCE, acrylic, and ceramic. Figure 4.9 shows responses of 0.6 ppm NH₃ measured by the 1 mg SnO₂ NFs@PANI that was cast on each substrate: acrylic, ceramic, SPCE, and SPGE. Noted here that during the sensor fabrication, low contact angle of a DMF drop containing sensing material was observed on the acrylic and ceramic substrates (Figure 4.10). This indicates poor contact between the SnO₂ NFs@PANI and the substrates which causes damage to the sensing material due to the extent of drop. Moreover, a slowly penetration of SnO₂ NFs@PANI was also found on both substrates revealing a loss of some sensing material from the substrate surface. These lead to low response of NH₃ gas and slow recovery time because the porous of sensing material and substrates were poor desorption for NH₃ gas. Compare to the SnO₂ NFs@PANI that was cast on the SPCE and SPGE substrates, higher responses were recorded as showed in Table 4.10, and fast recovery time due to the sensing material being a good adsorption and desorption NH₃ gas. This reveals a good contact between the substrates and SnO₂ NFs@PANI. No penetration of SnO₂ NFs@PANI was found on the SPCE and SPGE.

From these results, the SnO₂ NFs@PANI cast on the SPGE substrate gave the highest response to the NH₃ gas. Therefore, the SPGE was chosen as the substrate for SnO₂ NFs@PANI in DMF solution.

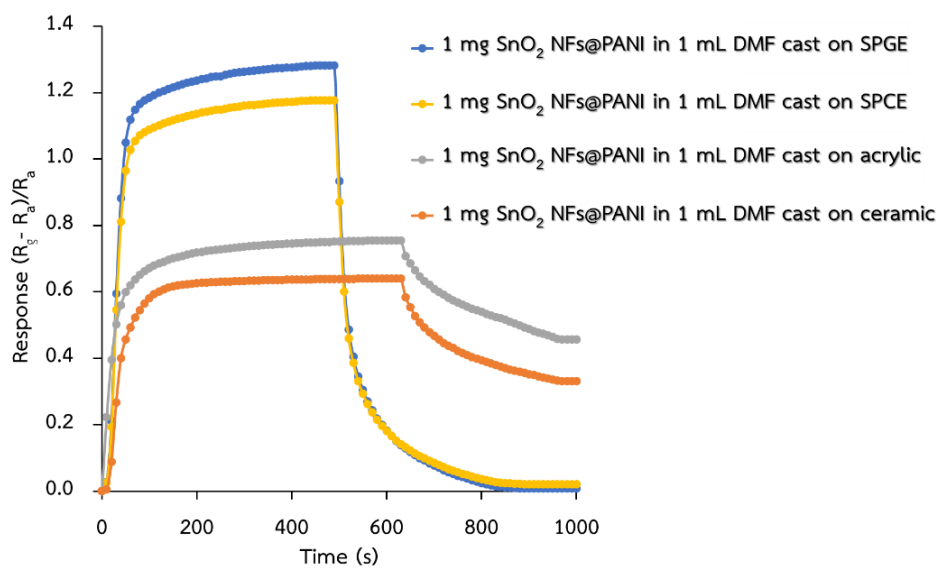


Figure 4.9 Responses of 0.6 ppm NH_3 measured by 1 mg SnO_2 NFs@PANI cast on acrylic (grey line), ceramic (orange line), SPCE (yellow line) and SPGE (blue line).

Table 4.10 Response of types of substrates.

Types of sensing material	Response				SD
	st 1	nd 2	rd 3	Average	
ceramic	0.70	0.63	0.59	0.64	0.04
acrylic	0.90	0.70	0.67	0.76	0.10
SPCE	1.14	1.18	1.22	1.18	0.03
SPGE	1.27	1.28	1.30	1.28	0.01

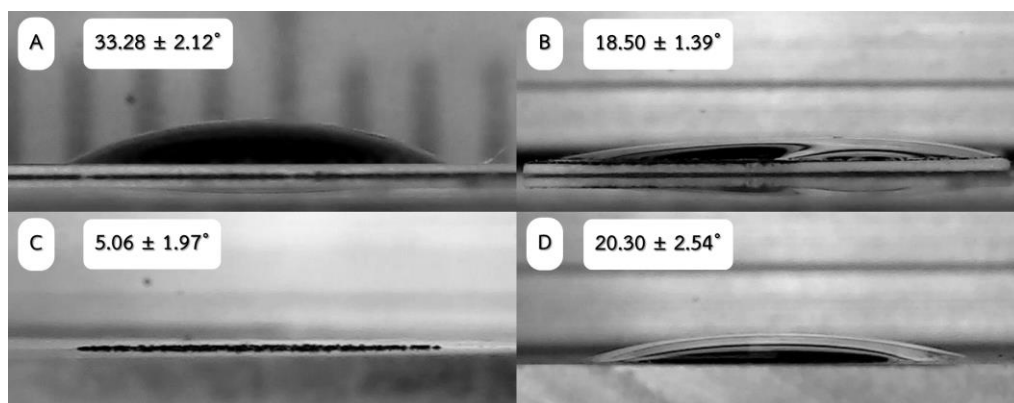


Figure 4.10 Contact angle of a DMF drop containing sensing material on difference substrate: A) SPGE, B) SPCE, C) ceramic, and D) acrylic.

4.3.3 Number of drop-casting layers

The number of drop-casting layers is very important for surface modification. The modifying layer is selected with the hope or anticipation of useful enhancement of the response towards some desired target analyte, via the adsorptive concentration of the target to analysis on the underlying substrate.

Drop-casting layers of 2 mg SnO₂ NFs@PANI sensing material were investigated. Figure 4.11 shows responses of 10 ppm NH₃ gas to the layers of 2, 4, 6, 8, and 10. A decrease in response was observed when the layer of the 2 mg SnO₂ NFs@PANI was increased from 2 to 6 layers due to the overlap surface area of sensing materials. However, the opposite trend was found when the layer increased from 6 to 10 due to the increase overlap surface area of the sensing material. As a result, the surface roughness was increased. Although, the high responses were found from the 10, 8, and 2 layers, respectively (Table 4.11), the consuming time to prepare those layers were much different. It took about 30, 24, and 3 mins to prepare the 10, 8, and 2 layers, respectively. Considering the ratio of response vs. preparation times (Table 4.12), 2 layers of the sensing material were chosen to be an appreciate layer.

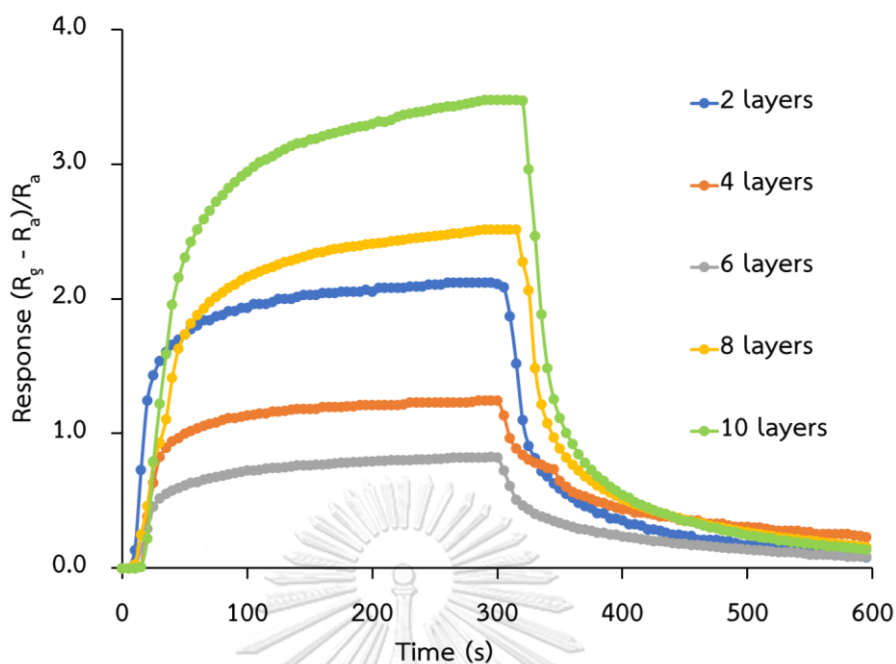


Figure 4.11 Responses of 10 ppm NH_3 measured by 2 mg SnO_2 NFs@PANI cast on SPGE with 2 layers (blue line), 4 layers (orange line), 6 layers (grey line), 8 layers (yellow line) and 10 layers (green line) drop casting.

Table 4.11 Response of drop-casting layers.

Types of sensing material	Response			Average	SD
	1 st	2 nd	3 rd		
2 layers	2.43	2.04	1.89	2.12	0.28
4 layers	1.97	0.96	0.81	1.25	0.63
6 layers	0.95	0.81	0.72	0.83	0.12
8 layers	2.60	2.48	2.47	2.51	0.07
10 layers	3.80	3.43	3.20	3.48	0.30

Table 4.12 Ratio of response vs. preparation times.

Number of layers	2 layers	4 layers	6 layers	8 layers	10 layers
Response, S	2.12	0.83	1.25	2.51	3.48
time (min.)	3	12	18	24	30
Ratio (S/t)	0.71	0.07	0.07	0.10	0.12

4.3.4 Concentration of SnO₂ NFs@PANI in DMF solution

Different concentrations of SnO₂ NFs@PANI; 1, 2, 5, and 7 mg in 1 mL DMF solution was cast on SPGE. Figure 4.12 shows responses of 10 ppm NH₃ measured by the sensor that contain each concentration of SnO₂ NFs@PANI that was cast on SPGE. An increase in the response was observed when 1, 2, and 5 mg SnO₂ NFs@PANI were applied was showed in Table 4.13. However, a decrease in response was found when 7 mg of SnO₂ NFs@PANI was used. This might be due to a decreased in active area caused by overlapping arrangements of the sensing material.

Thus, 5 mg SnO₂ NFs@PANI was chosen to be an optimized concentration for our sensor fabrication.

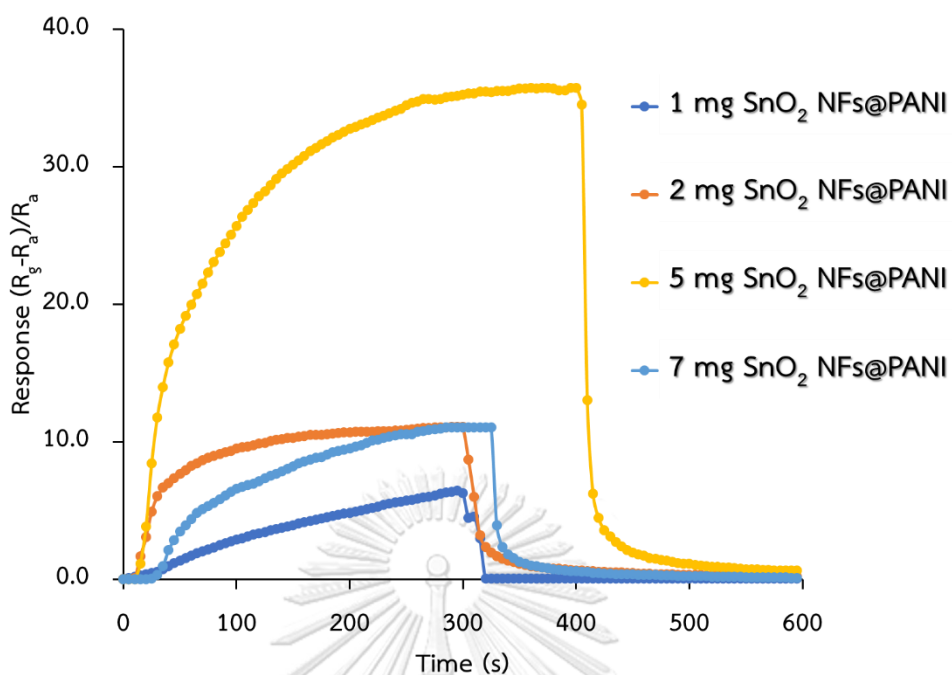


Figure 4.12 Responses of 10 ppm NH_3 measured by 1 mg (blue line), 2 mg (orange line), 5 mg (yellow line), and 7 mg (grey line) SnO_2 NFs@PANI cast on SPGE.

Table 4.13 Response of concentration of SnO_2 NFs@PANI in DMF solution.

Concentration of SnO_2 NFs@PANI	Response				SD
	1 st	2 nd	3 rd	Average	
1 mg	7.55	5.56	6.23	6.45	1.01
2 mg	11.19	11.54	10.58	11.11	0.48
5 mg	36.41	35.07	35.37	35.61	0.70
7 mg	11.19	11.55	11.14	11.29	0.22

4.4 Performance of NH₃ sensor

Ammonia sensing properties made of the SnO₂ NFs@PANI composite were investigated at room temperature. Linear range, limit of detection, selectivity, repeatability, long-term stability, reproducibility, and application of the fabricated SnO₂ NFs@PANI sensor were studied.

4.4.1 Linear range and limit of detection

Sensing performance of the SnO₂ NFs@PANI cast on the SPGE substrate was evaluated by monitoring the change of resistance for 0.4 - 100 ppm NH₃ gas at room temperature. Figure 4.13(A) shows that the response quickly rose up when the sensor was exposed to NH₃ gas and fell back to the initial value when the NH₃ gas was replaced by air. This behavior indicates a typical p-n junction of a semiconductor with excellent reversibility. The NH₃ concentration dependence was displayed in Figure 4.13(B). The SnO₂ NFs@PANI sensor has a NH₃ sensitivity of 17.243 per ppm, with a correlation coefficient (R^2) of 0.999. The results showed that the SnO₂ NFs@PANI sensor can detect NH₃ in a wide concentration range (0.4-100 ppm) which cover the limit of NH₃ to human (25 ppm for 8 hrs and 35 ppm for 15 mins) defined by the Occupational Safety and Health Administration (OSHA) (Pandeewari et al., 2022). The detection limit of SnO₂ NFs@PANI cast on SPGE substrate was calculated by method of detection limits (MDL) = 3SD/slope in which yields the detection limit of 0.0124 ppm (12.4 ppb) NH₃ gas.

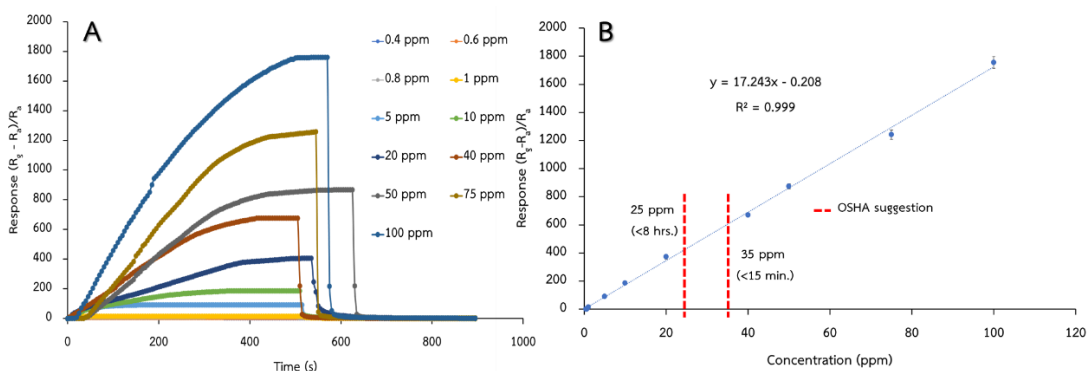


Figure 4.13 A) Dynamic response of the SnO₂ NFs@PANI sensor to 0.4 - 100 ppm NH₃ gas. B) Response of the SnO₂ NFs@PANI sensor as a function of NH₃ concentration at room temperature.

4.4.2 Selectivity

Selectivity of the SnO₂ NFs@PANI sensor was examined by 10 ppm of various gases: NH₃, acetone, ethanol, formaldehyde, methanol, and toluene gases at room temperature due to these gases are used in industries such as the agricultural industry, fertilizer production industry, cleaning products industry, pharmaceutical industry and plastic and polymer manufacturing industry (Arasu et al., 2017). The results summarized in Figure 4.14 clearly demonstrate the highest response on the NH₃ gas compared to the other gases. This indicates that the SnO₂ NFs@PANI sensor has an excellent selectivity toward the NH₃ gas.

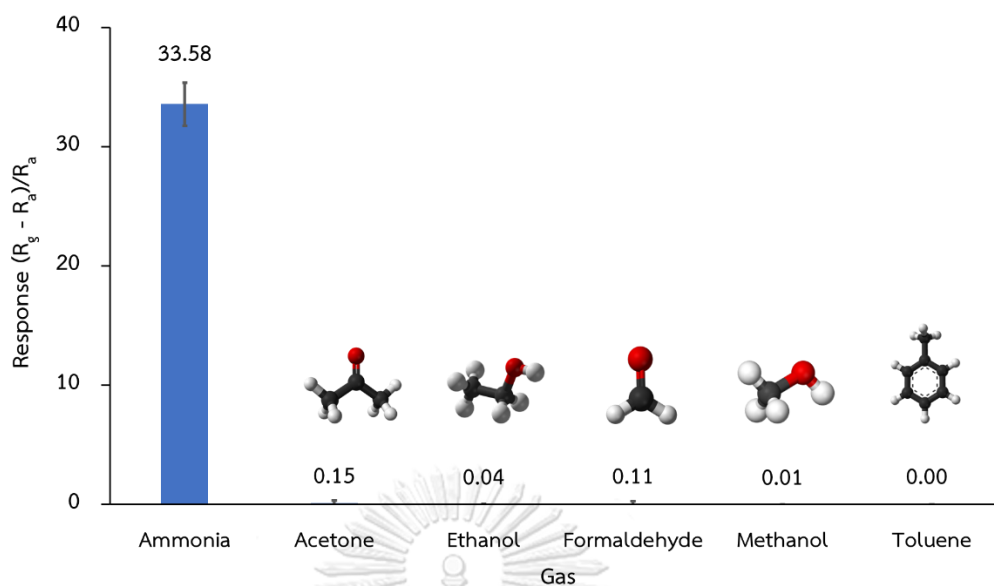


Figure 4.14 Selectivity responses of 10 ppm NH_3 , acetone, ethanol, formaldehyde, methanol, and toluene gases at room temperature.

4.4.3 Repeatability and long-term stability

Stability of the fabricated sensor, SnO_2 NFs@PANI cast on SPGE, was examined in terms of repeatability and long-term stability. Figure 4.15A shows ten repeatedly measurements of 10 ppm NH_3 gas. Small, fluctuated response (SD = 2.11) was observed in the result. The response quickly rose up when the sensor was exposed to NH_3 gas and fell back to the initial value when the NH_3 gas was replaced by air. Daily averaged responses of 10 ppm NH_3 gas measurement were plotted in Figure 4.15B. A slightly decreases in the response was found in the first seven days which could be due to the SnO_2 NFs@PANI film cannot completely release ammonia gas. aging and the disappearance of unstable adsorption sites (Pang et al., 2018; Xu & Wu, 2020). After day seventh, a stable response was observed for about 2 months. These results suggest good repeatability and long-term use of the SnO_2 NFs@PANI sensor.

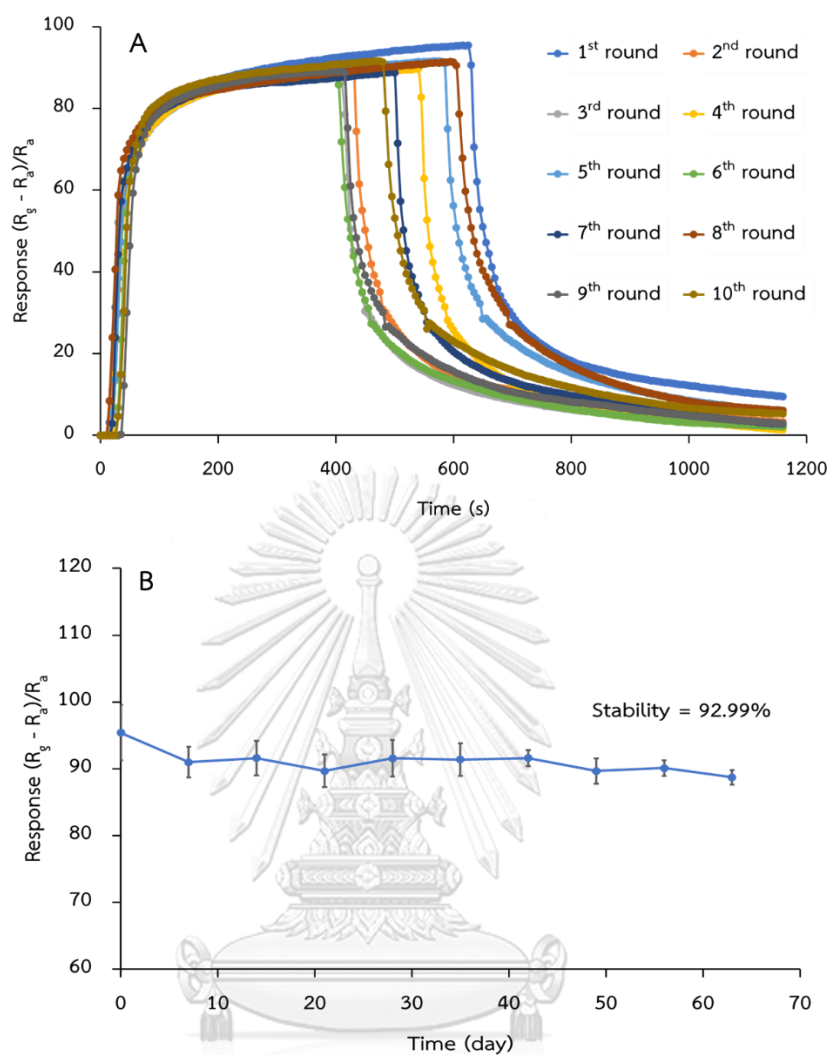


Figure 4.15 A) Ten repeatedly responses. B) Long-term stability of the SnO₂ NFs@PANI sensor response to 10 ppm NH₃ gas at room temperature.

4.4.4 Reproducibility

The reproducibility of the fabricated sensor, SnO₂ NFs@PANI cast on SPGE was summarized in Figure 4.16, which demonstrates the reproducibility response of five sensors to 10 ppm NH₃ gas. According to the result, all sensors gave a similar response, indicating that the sensor possesses good reproducibility to NH₃ gas detection with a relative standard deviation (%RSD) of 4.84 which is High production process reliability.

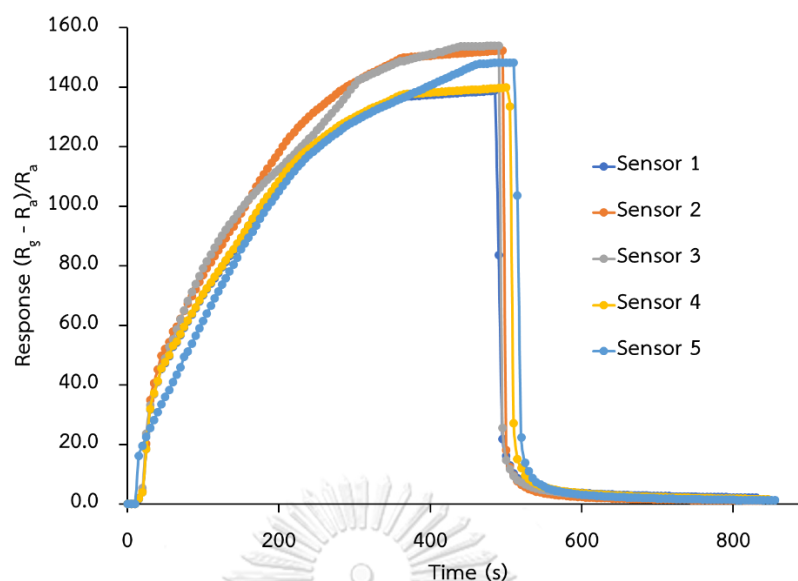


Figure 4.16 Reproducibility response of five SnO₂ NFs@PANI sensors to 10 ppm NH₃ gas at room temperature

Table 4.14 Response of fabricated sensor (reproducibility test)

Sensor	Response	Average response	SD	%RSD
1	139.12	147.22	7.12	4.84
2	152.51			
3	153.84			
4	139.92			
5	150.73			

4.4.5 Sample analysis

As the fabricated sensor, SnO₂ NFs@PANI cast on SPGE, shows a good performance in terms of LOD, selectivity and stability, it is possible to use this sensor for food-freshness monitoring in any containers or packages for long hours. Demonstration of the food-freshness monitoring was, then, illustrated in the following experiment. Fresh-fish filet stored in a close box represents food in container. NH₃ gas was monitored, by our fabricated sensor, every 1 hr at

room temperature and at refrigerator temperature (4 °C). With many hrs. storage, if the food rotten, high concentration of NH₃ gas in the container is expected. Figure 4.17 shows results of this experiment.

At room temperature, a slowly increase of NH₃ gas concentration was detected up to 1.82 ppm in the first 18 hrs. No change in color or smell from the fish fillet was observed. However, after the 18 hrs, a huge increase of NH₃ gas concentration was detected. Physically changes from the fish fillet, slightly color change and distinctly pungent smell, were notify by the 20th hrs., indicating a rotten point of the fish fillet. At this hr, 12.46 ppm NH₃ gas was detected.

For the other fish filter that was stored in refrigerator (4 °C), no big change in the NH₃ gas concentration, nor physically change from the fillet was detected during 0 - 18 hrs. The highest NH₃ concentration was 0.32 – 1.82 ppm which was much lower than the fish-fillet rotten point (12.46 ppm).

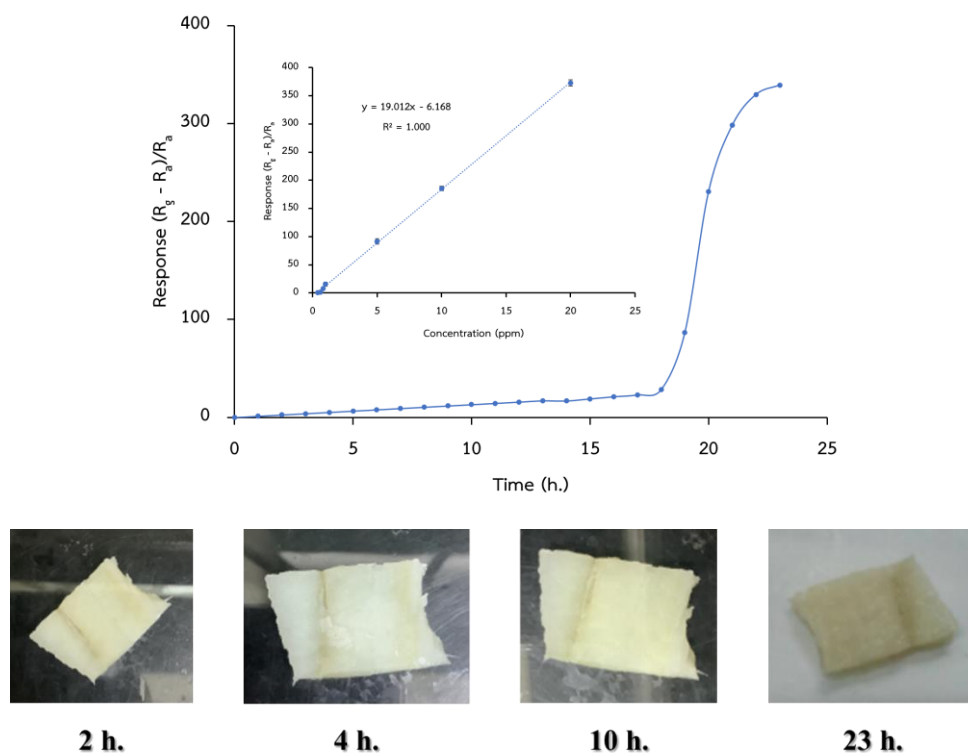


Figure 4.17 NH₃ contents in fish sample detected by the SnO₂ NFs@PANI sensor.

4.4.6 Summary of NH₃ sensing parameters for PANI-metal oxide-based sensing systems

There are several techniques for detecting NH₃ gas. The most widely used detection methods are the optical method (Mount et al., 2002; Peeters et al., 2000) (optical sensors utilizing tunable diode laser spectroscopy), electrochemical sensors (Xiong & Compton, 2014), surface acoustic wave sensors (Lin et al., 2011), field effect transistor sensors (Chen et al., 2012), and the solid-state probe analysis methods (Balint et al., 2014; Huang et al., 2009; Janata & Josowicz, 2003; Kim & Lee, 2014; Kwak et al., 2019) (metal oxide-based sensors, conducting polymer sensors, and conducting polymer-metal oxide composite sensors). The solid-state probe analysis method is one of the most widely used methods for the determination of NH₃ gas, as it is a simple, and low-cost method. However, there are many variations in the construction of a stable and analytical specificity. It is well known that PANI-metal oxide composite can be used to make NH₃ gas receptors at room temperature (Pandeewari et al., 2022). Based on the use of PANI as a conducting polymer, there are many types of conducting polymer-metal oxide sensors such as PANI- α -Fe₂O₃ (Bandgar, Navale, Naushad, et al., 2015; Bandgar et al., 2017; Chabukswar et al., 2019), PANI-SiO₂ (Zhang et al., 2020), PANI-TiO₂ (Zhu et al., 2018) and PANI-ZnO (Patil et al., 2012). Table 4.4 shows the comparisons for the sensing properties of SnO₂ NFs@PANI and previously reported devices. Quite clear that the SnO₂ NFs@PANI sensor exhibited the good sensing performance to NH₃ at room temperature comparing with previously reported devices. Hence, combined PANI with SnO₂ NFs could be an effective approach for improving the sensing response of sensors to the NH₃.

Table 4.15 Sensing performance of the recently reported NH₃ gas sensors base on PANI-metal oxide in advanced techniques.

Sensing Methods	LOD	Response/ recovery time	Response (R _g - R _a)/R _a	Operation temp.	Reference
PANI-CeO ₂	2 ppm	57.6 s/ -	6.5 (50 ppm)	RT	(Wang et al., 2014)
PANI-CuFe ₂ O ₄	1 ppm	84 s/ 54 s	0.27 (5 ppm)	20 °C	(X. Wang et al., 2020)
PANI-CuO	0.05 ppm	30 s/ -	9.30 (100 ppm)	25 ± 2 °C	(Ahmadi Tabar et al., 2020)
PANI-CuO-TiO ₂ -SiO ₂	0.4 ppm	-	45.67 (100 ppm)	RT	(Pang et al., 2017)
PANI- α -Fe ₂ O ₃	2.5 ppm	65 s/ 50 s	0.72 (100 ppm)	RT	(Bandgar et al., 2017)
PANI- α -Fe ₂ O ₃	1 ppm	26 s/ 25 s	0.43 (100 ppm)	RT	(Chabukswar et al., 2019)
PANI-SiO ₂	0.4 ppm	-	3.36 (5 ppm)	25 ± 1 °C	(Nie et al., 2018)
PANI-SrGe ₄ O ₉	250 ppt	62 s/ 223 s	0.16 (0.2 ppm)	25 ± 2 °C	(Zhang et al., 2020)
PANI-TiO ₂ -Au	10 ppm	52 s/ 180 s	1.23 (50 ppm)	25 °C	(Liu et al., 2017)
PANI-TiO ₂	0.5 ppm	100 s/ 232 s	5.4 (100 ppm)	20 ± 5 °C	(Zhu et al., 2018)
PANI-ZnO	10 ppm	22 s/ 418 s	0.28 (100 ppm)	27 °C	(Patil et al., 2012)
SnO ₂ NFs@PANI	12.4 ppb	87 s/ 160 s	1756 (100 ppm)	30 ± 5 °C	This work

CHAPTER 5

CONCLUSION

In this work, tin dioxide nanofibers@polyaniline nanocomposite (SnO_2 NFs@PANI) sensors were prepared and successfully fabricated by *in-situ* chemical oxidative polymerization for the detection of ammonia gas. The as-prepared nanocomposite was fully characterized through SEM, EDS, and XRD measurements. The gas-sensing properties of the SnO_2 NFs@PANI sensor for ammonia indicated that these nanocomposites were good candidates for the ammonia detection. The NH_3 -sensing performances of the sensors were evaluated at room temperature, which showed that the SnO_2 NFs@PANI sensor possessed improved response, short response/recovery times, perfect response-concentration linearity (0.4-100 ppm), good reproducibility, splendid selectivity, good long-term stability, low detectable concentration (0.4 ppm) and the limit of detection (12.4 ppb). The possible sensing mechanism of the SnO_2 NFs@PANI with better sensing properties was attributed to the formation of p-n hetero-junction between the PANI and SnO_2 . Therefore, the SnO_2 NFs@PANI with excellent NH_3 gas-sensing properties may have great promise in the application of food freshness evaluation.

REFERENCES

- Abu-Thabit, N. Y. (2016). Chemical oxidative polymerization of polyaniline: a practical approach for preparation of smart conductive textiles. *Journal of Chemical Education*, 93(9), 1606-1611.
- Ahmadi Tabar, F., Nikfarjam, A., Tavakoli, N., Nasrollah Gavgani, J., Mahyari, M., & Hosseini, S. G. (2020). Chemical-resistant ammonia sensor based on polyaniline/CuO nanoparticles supported on three-dimensional nitrogen-doped graphene-based framework nanocomposites. *Microchimica Acta*, 187(5), 293.
- Ai, X., Anderson, N., Guo, J., Kowalik, J., Tolbert, L. M., & Lian, T. (2006). Ultrafast photoinduced charge separation dynamics in polythiophene/SnO₂ nanocomposites. *The Journal of Physical Chemistry B*, 110(50), 25496-25503.
- Alfaro De Prá, M. A., Ribeiro-do-Valle, R. M., Maraschin, M., & Veleirinho, B. (2017). Effect of collector design on the morphological properties of polycaprolactone electrospun fibers. *Materials Letters*, 193, 154-157.
- Arasu, P. T., Khalaf, A. L., Aziz, S. H. A., Yaacob, M. H., & Noor, A. S. M. (2017, 14-16 July 2017). Optical fiber based ammonia gas sensor with carbon nanotubes sensing enhancement. 2017 IEEE Region 10 Symposium (TENSymp),
- Awang, Z. (2014). Gas sensors: A review. *Sens. Transducers*, 168(4), 61-75.
- Balint, R., Cassidy, N. J., & Cartmell, S. H. (2014). Conductive polymers: Towards a smart biomaterial for tissue engineering. *Acta Biomaterialia*, 10(6), 2341-2353.
- Bandara, T. M. W. J., Weerasinghe, A. M. J. S., Dissanayake, M. A. K. L., Senadeera, G. K. R., Furlani, M., Albinsson, I., & Mellander, B. E. (2018). Characterization of poly(vinylidene fluoride-co-hexafluoropropylene) (PVdF-HFP) nanofiber membrane based quasi solid electrolytes and their application in a dye sensitized solar cell. *Electrochimica Acta*, 266, 276-283.
- Bandgar, D. K., Navale, S. T., Nalage, S. R., Mane, R. S., Stadler, F. J., Aswal, D. K., Gupta, S. K., & Patil, V. B. (2015). Simple and low-temperature polyaniline-based flexible ammonia sensor: a step towards laboratory synthesis to economical device design. *Journal of Materials Chemistry C*, 3, 9461-9468.

- Bandgar, D. K., Navale, S. T., Naushad, M., Mane, R. S., Stadler, F. J., & Patil, V. B. (2015). Ultra-sensitive polyaniline–iron oxide nanocomposite room temperature flexible ammonia sensor [10.1039/C5RA11512D]. *RSC Advances*, 5(84), 68964-68971.
- Bandgar, D. K., Navale, S. T., Navale, Y. H., Ingole, S. M., Stadler, F. J., Ramgir, N., Aswal, D. K., Gupta, S. K., Mane, R. S., & Patil, V. B. (2017). Flexible camphor sulfonic acid-doped PAni/ α -Fe₂O₃ nanocomposite films and their room temperature ammonia sensing activity. *Materials Chemistry and Physics*, 189, 191-197.
- Bao, M., Wang, X., Yuan, H., Lou, X., Zhao, Q., & Zhang, Y. (2016). HAp incorporated ultrafine polymeric fibers with shape memory effect for potential use in bone screw hole healing [10.1039/C6TB01305H]. *Journal of Materials Chemistry B*, 4(31), 5308-5320.
- Bera, S., Kundu, S., Khan, H., & Jana, S. (2018). Polyaniline coated graphene hybridized SnO₂ nanocomposite: Low temperature solution synthesis, structural property and room temperature ammonia gas sensing. *Journal of Alloys and Compounds*, 744, 260-270.
- Beygisangchin, M., Abdul Rashid, S., Shafie, S., Sadrolhosseini, A. R., & Lim, H. N. (2021). Preparations, properties, and applications of polyaniline and polyaniline thin films—A review. *Polymers*, 13(12).
- Bhowmick, T., Ambardekar, V., Ghosh, A., Dewan, M., Bandyopadhyay, P. P., Nag, S., & Majumder, S. B. (2020). Multilayered and chemiresistive thin and thick film gas sensors for air quality monitoring. *Multilayer Thin Films*, 127.
- Chabukswar, V. V., Bora, M. A., Adhav, P. B., Diwate, B. B., & Salunke-Gawali, S. (2019). Ultra-fast, economical and room temperature operating ammonia sensor based on polyaniline/iron oxide hybrid nanocomposites. *Polymer Bulletin*, 76(12), 6153-6167.
- Chatterjee, K., Dhara, P., Ganguly, S., Kargupta, K., & Banerjee, D. (2013). Morphology dependent ammonia sensing with 5-sulfosalicylic acid doped nanostructured polyaniline synthesized by several routes. *Sensors and Actuators B: Chemical*, 181, 544-550.
- Chen, L., Vivier, E., Eling, C. J., Babra, T. S., Bouillard, J.-S. G., Adawi, A. M., Benoit, D. M., Hartl, F., Colquhoun, H. M., Efremova, O. A., & Greenland, B. W. (2018).

- Conjugated, rod-like viologen oligomers: Correlation of oligomer length with conductivity and photoconductivity. *Synthetic Metals*, 241, 31-38.
- Chen, M., Wang, C., Fang, W., Wang, J., Zhang, W., Jin, G., & Diao, G. (2013). Electrospinning of calixarene-functionalized polyacrylonitrile nanofiber membranes and application as an adsorbent and catalyst support. *Langmuir*, 29(38), 11858-11867.
- Chen, T. Y., Chen, H. I., Hsu, C. S., Huang, C. C., Chang, C. F., Chou, P. C., & Liu, W. C. (2012). On an ammonia gas sensor based on a Pt/AlGa_N heterostructure field-effect transistor. *IEEE Electron Device Letters*, 33(4), 612-614.
- Chiu, S.-W., & Tang, K.-T. (2013). Towards a chemiresistive sensor-integrated electronic nose: A review. *Sensors*, 13(10), 14214-14247.
- Cho, N. G., Yang, D. J., Jin, M.-J., Kim, H.-G., Tuller, H. L., & Kim, I.-D. (2011). Highly sensitive SnO₂ hollow nanofiber-based NO₂ gas sensors. *Sensors and Actuators B: Chemical*, 160(1), 1468-1472.
- Das, M., & Sarkar, D. (2017). One-pot synthesis of zinc oxide - polyaniline nanocomposite for fabrication of efficient room temperature ammonia gas sensor. *Ceramics International*, 43(14), 11123-11131.
- Ding, B., Kim, J., Miyazaki, Y., & Shiratori, S. (2004). Electrospun nanofibrous membranes coated quartz crystal microbalance as gas sensor for NH₃ detection. *Sensors and Actuators B: Chemical*, 101(3), 373-380.
- Fang, X., Ma, H., Xiao, S., Shen, M., Guo, R., Cao, X., & Shi, X. (2011). Facile immobilization of gold nanoparticles into electrospun polyethyleneimine/polyvinyl alcohol nanofibers for catalytic applications [10.1039/C0JM03987J]. *Journal of Materials Chemistry*, 21(12), 4493-4501.
- Feng, Q., Li, X., Wang, J., & Gaskov, A. M. (2016). Reduced graphene oxide (rGO) encapsulated Co₃O₄ composite nanofibers for highly selective ammonia sensors. *Sensors and Actuators B: Chemical*, 222, 864-870.
- Feng, S., Farha, F., Li, Q., Wan, Y., Xu, Y., Zhang, T., & Ning, H. (2019). Review on smart gas sensing technology. *Sensors*, 19(17).
- Fuh, Y.-K., & Hsu, H.-S. (2011). Fabrication of monolithic polymer nanofluidic channels via near-field electrospun nanofibers as sacrificial templates. *Journal of*

- Micro/Nanolithography, MEMS, and MOEMS*, 10(4), 043004.
- Ge, J., Zong, D., Jin, Q., Yu, J., & Ding, B. (2018). Biomimetic and superwetable nanofibrous skins for highly efficient separation of oil-in-water emulsions. *Advanced Functional Materials*, 28(10), 1705051.
- He, W., Zhao, Y., & Xiong, Y. (2020). Bilayer polyaniline- WO_3 thin-film sensors sensitive to NO_2 . *ACS Omega*, 5(17), 9744-9751.
- Hoa, N. D., Le, D. T. T., Tam, P. D., Le, A.-T., & Van Hieu, N. (2010). On-chip fabrication of SnO_2 -nanowire gas sensor: The effect of growth time on sensor performance. *Sensors and Actuators B: Chemical*, 146(1), 361-367.
- Hodgkinson, J., & Tatam, R. P. (2013). Optical gas sensing: a review. *Measurement Science and Technology*, 24(1), 012004.
- Hu, D., Huang, Y., Liu, H., Wang, H., Wang, S., Shen, M., Zhu, M., & Shi, X. (2014). The assembly of dendrimer-stabilized gold nanoparticles onto electrospun polymer nanofibers for catalytic applications [10.1039/C3TA13966B]. *Journal of Materials Chemistry A*, 2(7), 2323-2332.
- Huang, J., Wang, J., Gu, C., Yu, K., Meng, F., & Liu, J. (2009). A novel highly sensitive gas ionization sensor for ammonia detection. *Sensors and Actuators A: Physical*, 150(2), 218-223.
- Ibanez, J. G., Rincón, M. E., Gutierrez-Granados, S., Chahma, M. h., Jaramillo-Quintero, O. A., & Frontana-Urbe, B. A. (2018). Conducting polymers in the fields of energy, environmental remediation, and chemical-chiral sensors. *Chemical Reviews*, 118(9), 4731-4816.
- Janata, J., & Josowicz, M. (2003). Conducting polymers in electronic chemical sensors. *Nature Materials*, 2(1), 19-24.
- Jia, A., Liu, B., Liu, H., Li, Q., & Yun, Y. (2020). Interface Design of SnO_2 @PANI Nanotube With Enhanced Sensing Performance for Ammonia Detection at Room Temperature [Original Research]. *Frontiers in Chemistry*, 8.
- Ju, D., Xu, H., Qiu, Z., Guo, J., Zhang, J., & Cao, B. (2014). Highly sensitive and selective triethylamine-sensing properties of nanosheets directly grown on ceramic tube by forming NiO/ZnO PN heterojunction. *Sensors and Actuators B: Chemical*, 200, 288-296.

- Ju, D., Xu, H., Xu, Q., Gong, H., Qiu, Z., Guo, J., Zhang, J., & Cao, B. (2015). High triethylamine-sensing properties of NiO/SnO₂ hollow sphere P-N heterojunction sensors. *Sensors and Actuators B: Chemical*, 215, 39-44.
- K, N., & Rout, C. S. (2021). Conducting polymers: a comprehensive review on recent advances in synthesis, properties and applications [10.1039/D0RA07800J]. *RSC Advances*, 11(10), 5659-5697.
- Khattab, T. A., Abdelmoez, S., & Klapötke, T. M. (2016). Electrospun nanofibers from a tricyanofuran-based molecular switch for colorimetric recognition of ammonia gas. *Chemistry – A European Journal*, 22(12), 4157-4163.
- Kim, H.-J., & Lee, J.-H. (2014). Highly sensitive and selective gas sensors using p-type oxide semiconductors: Overview. *Sensors and Actuators B: Chemical*, 192, 607-627.
- Kumar, L., Rawal, I., Kaur, A., & Annapoorni, S. (2017). Flexible room temperature ammonia sensor based on polyaniline. *Sensors and Actuators B: Chemical*, 240, 408-416.
- Kumar, V., Mirzaei, A., Bonyani, M., Kim, K.-H., Kim, H. W., & Kim, S. S. (2020). Advances in electrospun nanofiber fabrication for polyaniline (PANI)-based chemoresistive sensors for gaseous ammonia. *TrAC Trends in Analytical Chemistry*, 129, 115938.
- Kwak, D., Lei, Y., & Maric, R. (2019). Ammonia gas sensors: A comprehensive review. *Talanta*, 204, 713-730.
- Kwon, O. S., Park, E., Kweon, O. Y., Park, S. J., & Jang, J. (2010). Novel flexible chemical gas sensor based on poly(3,4-ethylenedioxythiophene) nanotube membrane. *Talanta*, 82(4), 1338-1343.
- Lee, S. J., Heo, D. N., Moon, J.-H., Ko, W.-K., Lee, J. B., Bae, M. S., Park, S. W., Kim, J. E., Lee, D. H., Kim, E.-C., Lee, C. H., & Kwon, I. K. (2014). Electrospun chitosan nanofibers with controlled levels of silver nanoparticles. Preparation, characterization and antibacterial activity. *Carbohydrate Polymers*, 111, 530-537.
- Li, D., & Xia, Y. (2004). Electrospinning of nanofibers: Reinventing the wheel?. *Advanced Materials*, 16(14), 1151-1170.
- Li, S., Diao, Y., Yang, Z., He, J., Wang, J., Liu, C., Liu, F., Lu, H., Yan, X., Sun, P., & Lu, G. (2018). Enhanced room temperature gas sensor based on Au-loaded mesoporous

- In₂O₃ nanospheres@polyaniline core-shell nanohybrid assembled on flexible PET substrate for NH₃ detection. *Sensors and Actuators B: Chemical*, 276, 526-533.
- Li, S., Wang, T., Yang, Z., He, J., Wang, J., Zhao, L., Lu, H., Tian, T., Liu, F., Sun, P., Yan, X., & Lu, G. (2018). Room temperature high performance NH₃ sensor based on GO-rambutan-like polyaniline hollow nanosphere hybrid assembled to flexible PET substrate. *Sensors and Actuators B: Chemical*, 273, 726-734.
- Li, Y., Ban, H., & Yang, M. (2016). Highly sensitive NH₃ gas sensors based on novel polypyrrole-coated SnO₂ nanosheet nanocomposites. *Sensors and Actuators B: Chemical*, 224, 449-457.
- Likhar, P. R., Arundhathi, R., Ghosh, S., & Kantam, M. L. (2009). Polyaniline nanofiber supported FeCl₃ : An efficient and reusable heterogeneous catalyst for the acylation of alcohols and amines with acetic acid. *Journal of Molecular Catalysis A: Chemical*, 302(1), 142-149.
- Lin, T. H., Li, Y. T., Hao, H. C., Fang, I. C., Yang, C. M., & Yao, D. J. (2011, 5-9 June 2011). Surface acoustic wave gas sensor for monitoring low concentration ammonia. 2011 16th International Solid-State Sensors, Actuators and Microsystems Conference,
- Liu, C., Tai, H., Zhang, P., Ye, Z., Su, Y., & Jiang, Y. (2017). Enhanced ammonia-sensing properties of PANI-TiO₂-Au ternary self-assembly nanocomposite thin film at room temperature. *Sensors and Actuators B: Chemical*, 246, 85-95.
- Liu, C., Tai, H., Zhang, P., Yuan, Z., Du, X., Xie, G., & Jiang, Y. (2018). A high-performance flexible gas sensor based on self-assembled PANI-CeO₂ nanocomposite thin film for trace-level NH₃ detection at room temperature. *Sensors and Actuators B: Chemical*, 261, 587-597.
- Liu, H., Xu, M., Wei, C., Ma, W., Wang, Y., Gan, R., Ma, C., & Shi, J. (2021). SnCl₂-induced SnO₂ nanoparticles uniformly anchored in the interpenetrating network porous structure of electrode-membranes to relieve volume expansion and enhance lithium storage performance. *Colloids and Surfaces A: Physicochemical and Engineering Aspects*, 628, 127348.
- Liu, H., Zhang, L., Li, K. H., & Tan, O. K. (2018). Microhotplates for metal oxide semiconductor gas sensor applications—Towards the CMOS-MEMS monolithic

- approach. *Micromachines*, 9(11).
- Liu, Y., Hao, M., Chen, Z., Liu, L., Liu, Y., Yang, W., & Ramakrishna, S. (2020). A review on recent advances in application of electrospun nanofiber materials as biosensors. *Current Opinion in Biomedical Engineering*, 13, 174-189.
- Liu, Y., Zhang, L., Sun, X.-F., Liu, J., Fan, J., & Huang, D.-W. (2015). Multi-jet electrospinning via auxiliary electrode. *Materials Letters*, 141, 153-156.
- Ma, G., Fang, D., Liu, Y., Zhu, X., & Nie, J. (2012). Electrospun sodium alginate/poly(ethylene oxide) core-shell nanofibers scaffolds potential for tissue engineering applications. *Carbohydrate Polymers*, 87(1), 737-743.
- Manesh, K. M., Santhosh, P., Gopalan, A., & Lee, K.-P. (2007). Electrospun poly(vinylidene fluoride)/poly(aminophenylboronic acid) composite nanofibrous membrane as a novel glucose sensor. *Analytical Biochemistry*, 360(2), 189-195.
- Matthews, J. A., Wnek, G. E., Simpson, D. G., & Bowlin, G. L. (2002). Electrospinning of collagen nanofibers. *Biomacromolecules*, 3(2), 232-238.
- Mazzeu, M. A. C., Faria, L. K., Baldan, M. R., Rezende, M. C., & Gonçalves, E. S. (2018). Influence of reaction time on the structure of polyaniline synthesized on a pre-pilot scale. *Brazilian Journal of Chemical Engineering*, 35, 123-130.
- Mikhaylov, S., Ogurtsov, N., Noskov, Y., Redon, N., Coddeville, P., Wojkiewicz, J. L., & Pud, A. (2015). Ammonia/amine electronic gas sensors based on hybrid polyaniline-TiO₂ nanocomposites. The effects of titania and the surface active doping acid [10.1039/C4RA16121A]. *RSC Advances*, 5(26), 20218-20226.
- Mikołajczyk, J., Magryta, P., Stacewicz, T., Smulko, J., Bielecki, Z., Wojtas, J., Szabra, D., Lentka, Ł., & Prokopiuk, A. (2016). Detection of gaseous compounds with different techniques. *Metrology and Measurement Systems*, vol. 23(No 2), 205-224.
- Mount, G. H., Rumburg, B., Havig, J., Lamb, B., Westberg, H., Yonge, D., Johnson, K., & Kincaid, R. (2002). Measurement of atmospheric ammonia at a dairy using differential optical absorption spectroscopy in the mid-ultraviolet. *Atmospheric Environment*, 36(11), 1799-1810.
- Nezakati, T., Seifalian, A., Tan, A., & Seifalian, A. M. (2018). Conductive polymers: Opportunities and challenges in biomedical applications. *Chemical Reviews*,

118(14), 6766-6843.

- Nicolas-Debarnot, D., & Poncin-Epaillard, F. (2003). Polyaniline as a new sensitive layer for gas sensors. *Analytica Chimica Acta*, 475(1), 1-15.
- Nie, Q., Pang, Z., Li, D., Zhou, H., Huang, F., Cai, Y., & Wei, Q. (2018). Facile fabrication of flexible SiO₂/PANI nanofibers for ammonia gas sensing at room temperature. *Colloids and Surfaces A: Physicochemical and Engineering Aspects*, 537, 532-539.
- Pandeewari, R., Jeyaprakash, B. G., Veluswamy, P., & Balamurugan, D. (2022). Enhanced selective ammonia detection of spray deposited Cd-doped β -Ga₂O₃ thin films with low hysteresis effect. *Ceramics International*, 48(19, Part B), 29067-29080.
- Pang, Z., Fu, J., Luo, L., Huang, F., & Wei, Q. (2014). Fabrication of PA6/TiO₂/PANI composite nanofibers by electrospinning-electrospraying for ammonia sensor. *Colloids and Surfaces A: Physicochemical and Engineering Aspects*, 461, 113-118.
- Pang, Z., Nie, Q., Lv, P., Yu, J., Huang, F., & Wei, Q. (2017). Design of flexible PANI-coated CuO-TiO₂-SiO₂ heterostructure nanofibers with high ammonia sensing response values. *Nanotechnology*, 28(22), 225501.
- Pang, Z., Yu, J., Li, D., Nie, Q., Zhang, J., & Wei, Q. (2018). Free-standing TiO₂-SiO₂/PANI composite nanofibers for ammonia sensors. *Journal of Materials Science: Materials in Electronics*, 29(5), 3576-3583.
- Patil, S. L., Chougule, M. A., Sen, S., & Patil, V. B. (2012). Measurements on room temperature gas sensing properties of CSA doped polyaniline-ZnO nanocomposites. *Measurement*, 45(3), 243-249.
- Peeters, R., Berden, G., Apituley, A., & Meijer, G. (2000). Open-path trace gas detection of ammonia based on cavity-enhanced absorption spectroscopy. *Applied Physics B*, 71(2), 231-236.
- Persano, L., Camposeo, A., Tekmen, C., & Pisignano, D. (2013). Industrial upscaling of electrospinning and applications of polymer nanofibers: A review. *Macromolecular Materials and Engineering*, 298(5), 504-520.
- Pinto, N. J., Ramos, I., Rojas, R., Wang, P.-C., & Johnson, A. T. (2008). Electric response of isolated electrospun polyaniline nanofibers to vapors of aliphatic alcohols. *Sensors and Actuators B: Chemical*, 129(2), 621-627.

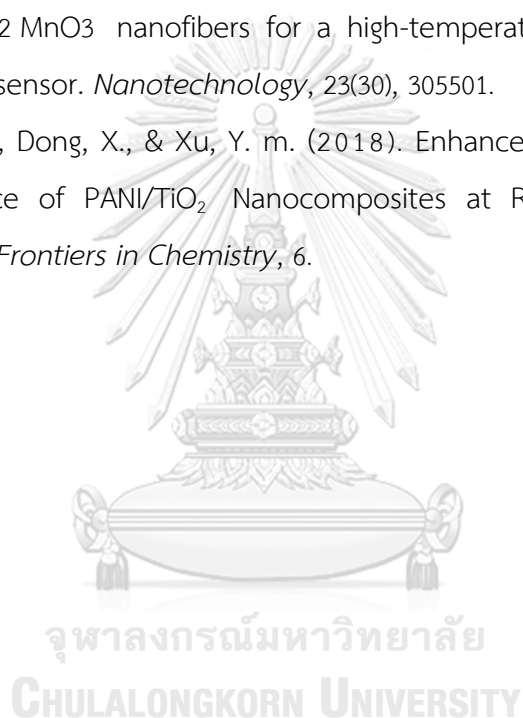
- Qayum, A., Wei, J., Li, Q., Chen, D., Jiao, X., & Xia, Y. (2019). Efficient decontamination of multi-component wastewater by hydrophilic electrospun PAN/AgBr/Ag fibrous membrane. *Chemical Engineering Journal*, 361, 1255-1263.
- Rim, N. G., Shin, C. S., & Shin, H. (2013). Current approaches to electrospun nanofibers for tissue engineering. *Biomedical Materials*, 8(1), 014102.
- Sanjeeda, I., & Taiyaba, A. N. (2014). Natural dyes: their sources and ecofriendly use as textile materials. *Journal of Environmental Research and development*, 8(3A), 683.
- Shaalan, N. M., Hamad, D., Aljaafari, A., Abdel-Latif, A. Y., & Abdel-Rahim, M. A. (2019). Preparation and characterization of developed $\text{Cu}_x\text{Sn}_{1-x}\text{O}_2$ nanocomposite and its promising methane gas sensing properties. *Sensors*, 19(10).
- Su, P. G., Lee, C. T., & Chou, C. Y. (2009). Flexible NH_3 sensors fabricated by in situ self-assembly of polypyrrole. *Talanta*, 80(2), 763-769.
- Sui, L.-l., Xu, Y.-M., Zhang, X.-F., Cheng, X.-L., Gao, S., Zhao, H., Cai, Z., & Huo, L.-H. (2015). Construction of three-dimensional flower-like $\alpha\text{-MoO}_3$ with hierarchical structure for highly selective triethylamine sensor. *Sensors and Actuators B: Chemical*, 208, 406-414.
- Sundarrajan, S., & Ramakrishna, S. (2007). Fabrication of nanocomposite membranes from nanofibers and nanoparticles for protection against chemical warfare stimulants. *Journal of Materials Science*, 42(20), 8400-8407.
- Sung, M.-T., Chang, M.-H., & Ho, M.-H. (2014). Investigation of cathode electrocatalysts composed of electrospun Pt nanowires and Pt/C for proton exchange membrane fuel cells. *Journal of Power Sources*, 249, 320-326.
- Syrový, T., Kuberský, P., Sapurina, I., Pretl, S., Bober, P., Syrová, L., Hamáček, A., & Stejskal, J. (2016). Gravure-printed ammonia sensor based on organic polyaniline colloids. *Sensors and Actuators B: Chemical*, 225, 510-516.
- Tai, H., Jiang, Y., Xie, G., Yu, J., & Chen, X. (2007). Fabrication and gas sensitivity of polyaniline-titanium dioxide nanocomposite thin film. *Sensors and Actuators B: Chemical*, 125(2), 644-650.
- Tanguy, N. R., Thompson, M., & Yan, N. (2018). A review on advances in application of polyaniline for ammonia detection. *Sensors and Actuators B: Chemical*, 257,

1044-1064.

- Tran, V. V., Nu, T. T., Jung, H.-R., & Chang, M. (2021). Advanced photocatalysts based on conducting polymer/metal oxide composites for environmental applications. *Polymers*, 13(18).
- Unnithan, A. R., Gnanasekaran, G., Sathishkumar, Y., Lee, Y. S., & Kim, C. S. (2014). Electrospun antibacterial polyurethane–cellulose acetate–zein composite mats for wound dressing. *Carbohydrate Polymers*, 102, 884-892.
- Valipouri, A. (2017). Production scale up of nanofibers: a review. *Journal of Textiles and Polymers*, 5(1), 8-16.
- Van Hieu, N. (2010). Comparative study of gas sensor performance of SnO₂ nanowires and their hierarchical nanostructures. *Sensors and Actuators B: Chemical*, 150(1), 112-119.
- Wang, H., Gao, P., Lu, S., Liu, H., Yang, G., Pinto, J., & Jiang, X. (2011). The effect of tin content to the morphology of Sn/carbon nanofiber and the electrochemical performance as anode material for lithium batteries. *Electrochimica Acta*, 58, 44-51.
- Wang, L., Huang, H., Xiao, S., Cai, D., Liu, Y., Liu, B., Wang, D., Wang, C., Li, H., Wang, Y., Li, Q., & Wang, T. (2014). Enhanced Sensitivity and Stability of Room-Temperature NH₃ Sensors Using Core–Shell CeO₂ Nanoparticles@Cross-linked PANI with p–n Heterojunctions. *ACS Applied Materials & Interfaces*, 6(16), 14131-14140.
- Wang, W., Zhen, Y., Zhang, J., Li, Y., Zhong, H., Jia, Z., Xiong, Y., Xue, Q., Yan, Y., Alharbi, N. S., & Hayat, T. (2020). SnO₂ nanoparticles-modified 3D-multilayer MoS₂ nanosheets for ammonia gas sensing at room temperature. *Sensors and Actuators B: Chemical*, 321, 128471.
- Wang, X., Cui, F., Lin, J., Ding, B., Yu, J., & Al-Deyab, S. S. (2012). Functionalized nanoporous TiO₂ fibers on quartz crystal microbalance platform for formaldehyde sensor. *Sensors and Actuators B: Chemical*, 171-172, 658-665.
- Wang, X., Gong, L., Zhang, D., Fan, X., Jin, Y., & Guo, L. (2020). Room temperature ammonia gas sensor based on polyaniline/copper ferrite binary nanocomposites. *Sensors and Actuators B: Chemical*, 322, 128615.
- Wang, X., Zheng, G., Xu, L., Cheng, W., Xu, B., Huang, Y., & Sun, D. (2012). Fabrication of

- nanochannels via near-field electrospinning. *Applied Physics A*, 108(4), 825-828.
- Warland, J. S., Dias, G. M., & Thurtell, G. W. (2001). A tunable diode laser system for ammonia flux measurements over multiple plots. *Environmental Pollution*, 114(2), 215-221.
- Webber, M. E., Baer, D. S., & Hanson, R. K. (2001). Ammonia monitoring near 1.5 μm with diode-laser absorption sensors. *Applied Optics*, 40(12), 2031-2042.
- Wilson, A. D., & Baietto, M. (2009). Applications and Advances in Electronic-Nose Technologies. *Sensors*, 9(7), 5099-5148.
- Wu, R.-A., Wei Lin, C., & Tseng, W. J. (2017). Preparation of electrospun Cu-doped α -Fe₂O₃ semiconductor nanofibers for NO₂ gas sensor. *Ceramics International*, 43, S535-S540.
- Wu, W. (2019). Stretchable electronics: functional materials, fabrication strategies and applications. *Science and Technology of Advanced Materials*, 20(1), 187-224.
- Xiong, L., & Compton, R. G. (2014). Amperometric gas detection: A review. *Int. J. Electrochem. Sci*, 9(12), 7152-7181.
- Xu, L.-H., & Wu, T.-M. (2020). Synthesis of highly sensitive ammonia gas sensor of polyaniline/graphene nanoribbon/indium oxide composite at room temperature. *Journal of Materials Science: Materials in Electronics*, 31(9), 7276-7283.
- Xue, J., Xie, J., Liu, W., & Xia, Y. (2017). Electrospun nanofibers: New concepts, materials, and applications. *Accounts of Chemical Research*, 50(8), 1976-1987.
- Yan, Y., Yang, G., Xu, J.-L., Zhang, M., Kuo, C.-C., & Wang, S.-D. (2020). Conducting polymer-inorganic nanocomposite-based gas sensors: a review. *Science and Technology of Advanced Materials*, 21(1), 768-786.
- Yang, W., Chen, J., Zhu, G., Wen, X., Bai, P., Su, Y., Lin, Y., & Wang, Z. (2013). Harvesting vibration energy by a triple-cantilever based triboelectric nanogenerator. *Nano Research*, 6(12), 880-886.
- Yang, Y., Zhang, W., Yang, F., Brown, D. E., Ren, Y., Lee, S., Zeng, D., Gao, Q., & Zhang, X. (2016). Versatile nickel-tungsten bimetallics/carbon nanofiber catalysts for direct conversion of cellulose to ethylene glycol [10.1039/C6GC00703A]. *Green Chemistry*, 18(14), 3949-3955.

- Yuriar-Arredondo, K., Armstrong, M. R., Shan, B., Zeng, W., Xu, W., Jiang, H., & Mu, B. (2018). Nanofiber-based Matrimid organogel membranes for battery separator. *Journal of Membrane Science*, 546, 158-164.
- Zhang, Y., Zhang, J., Jiang, Y., Duan, Z., Liu, B., Zhao, Q., Wang, S., Yuan, Z., & Tai, H. (2020). Ultrasensitive flexible NH_3 gas sensor based on polyaniline/ SrGe_4O_9 nanocomposite with ppt-level detection ability at room temperature. *Sensors and Actuators B: Chemical*, 319, 128293.
- Zhi, M., Koneru, A., Yang, F., Manivannan, A., Li, J., & Wu, N. (2012). Electrospun $\text{La}_{0.8}\text{Sr}_{0.2}\text{MnO}_3$ nanofibers for a high-temperature electrochemical carbon monoxide sensor. *Nanotechnology*, 23(30), 305501.
- Zhu, C., Cheng, X., Dong, X., & Xu, Y. m. (2018). Enhanced Sub-ppm NH_3 Gas Sensing Performance of PANI/ TiO_2 Nanocomposites at Room Temperature [Original Research]. *Frontiers in Chemistry*, 6.



VITA

NAME Mr. Nattawut Soibang

DATE OF BIRTH 7 June 1994

PLACE OF BIRTH Lopburi

INSTITUTIONS ATTENDED Bachelor's Degree in Chemistry from Faculty of Science and Technology, Suan Sunandha Rajabhat University

HOME ADDRESS 352 Soi 13 Senavilla 84 Village, Khlongchan Subdistrict, Bangkok District, Bangkok 10240

